공학박사학위논문

유기발광 디스플레이 수명 모델 제안 및 모델 검증 체계 연구

Bivariate Lifetime Model and Validation Procedure for Organic Light-Emitting Diode Displays

2018년 2월

서울대학교 대학원

기계항공공학부

김 대 환

Abstract

Bivariate Lifetime Model and Validation Procedure for Organic Light-Emitting Diode Displays

Dae Whan Kim

Department of Mechanical and Aerospace Engineering

The Graduate School

Seoul National University

Despite the advantages of organic light-emitting diode (OLED) displays over liquid crystal displays, OLED displays suffer from reliability concerns related to luminance degradation and color shift. In particular, existing testing schemes are unable to reliably estimate the lifetime of large OLED displays (i.e., displays of 55 inches or larger). The limited number of test samples and the immature technology result in great hurdles for timely product development.

This study proposes a statistical approach to develop a lifetime model for OLED panels. The proposed approach incorporates manufacturing and operational uncertainties, and accurately estimates the lifetime of the OLED panels under normal usage conditions. The proposed statistical analysis approach consists of: (1) design of accelerated degradation tests (ADTs) for OLED panels, (2) establishment of a systematic scheme to build bivariate lifetime models for OLED panels, (3) development of two bivariate lifetime models for

OLED panels, and (4) statistical model validation for the heat dissipation analysis model for OLED TV design. This four-step statistical approach will help enable accurate lifetime prediction for large OLED panels subjected to various uncertainties. Thereby, this approach will foster efficient and effective OLED TV design to meet desired lifespan requirements.

Furthermore, two bivariate acceleration models are proposed in this research to estimate the lifetime of OLED panels under real-world usage conditions, subject to manufacturing and operational uncertainties. These bivariate acceleration models take into account two main factors—temperature and initial luminance intensity. The first bivariate acceleration model estimates the luminance degradation of the OLED panel; the second estimates the panel's color shift. The lifespan predicted by the proposed lifetime model shows a good agreement with experimental results.

Ensuring the color shift lifetime is a great hurdle for OLED product development. However, at present, there is no effective way to estimate the color shift lifetime at the early stages of product development while the product design is still changing. The research described here proposes a novel scheme for color shift lifetime analysis. The proposed method consists of: (1) a finite element model for OLED thermal analysis that incorporates the uncertainty of the measured surface temperature, (2) statistical model validation, including model calibration, to verify agreement between the predicted results and a set of experimental data (achieved through adjustment of a set of physical input variables and hypothesis tests for validity checking to measure the degree of mismatch between the predicted and observed results), and (3) a regression model that can predict the color shift lifetime using the surface temperature at the early stages of product

development. It is expected that the regression model can substantially shorten the product development time by predicting the color shift lifetime through OLED thermal analysis.

Keywords: Organic Light-Emitting Diode (OLED)
Accelerated Degradation Test (ADT)
Lifetime Model
Color Shift
Statistical Model Validation

Student Number: 2011-30198

Contents

Abstract i

Contents iv

List of Tables vii

List of Figures ix

Nomenclature xiii

Chapter 1. Introduction 1

1.1 Background and Motivation 1

1.2 Overview and Significance 2

1.3 Thesis Layout 6

Chapter 2. Literature Review 8

2.1 Accelerated Testing 8

2.2 Luminance Degradation Model for OLEDs 12

2.3 Color Shift of OLEDs 14

2.4 Verification and Validation Methodology 16

Chapter 3. OLED Degradation 28

3.1 Chromaticity and the Definition of Color Shift Lifetime 30

3.2 Degradation Mechanism 31

3.2.1 Luminance Degradation Mechanism 33

3.2.2 Color Shift Mechanism 34

3.3 Performance Degradation Models 36

3.3.1 Performance Degradation Model 36
3.3.2 Performance Color Shift Model 38
3.4 Acceleration Model 38

Chapter 4. Acceleration Degradation Testing (ADT) for OLEDs 42

4.1 Experimental Setup 42
4.2 Definition of the Time to Failure 46
4.2.1 The Time to Failure of Luminance 46
4.2.2 The Time to Failure of Color Shift 47
4.3 Lifespan Test Results 50

Chapter 5. Bivariate Lifetime Model for OLEDs 53

5.1 Fitting TTF Data to the Statistical Distribution 53
5.1.1 Estimation of Lifetime Distribution Parameters 53
5.1.2 Estimation of the Common Shape Parameter 58
5.1.3 Likelihood-Ratio Analysis 62
5.2 Bivariate Lifetime Model 64
5.2.1 Luminance Lifetime Model 64
5.2.2 Color Shift Lifetime Model 66
5.3 Validation of the Lifetime Model 67

Chapter 6. Statistical Model Validation of Heat Dissipation Analysis Model 77

6.1 Estimation Method for TTF using Surface Temperature 79
6.2 Thermal Analysis Model for OLED Displays 81
6.3 Statistical Calibration using the EDR Method 82
6.4 Validity Check 87
6.5 Results and Discussion 90

Chapter 7. Case Study 93

7.1 Computational Modeling 93
7.2 Estimation of Color Shift 95
7.3 Estimation of Luminance Degradation 96

Chapter 8. Contributions and Future Work 98

8.1 Contributions and Impacts 98
8.2 Suggestions for Future Research..... 103

References 104

Abstract (Korean) 116

List of Tables

Table 3-1 13^{th} MacAdam ellipse parameters 32

Table 4-1 Description of the display pattern in each TV set 43

Table 5-1 Goodness-of-fit test results of luminance TTFs 55

Table 5-2 Goodness-of-fit test results of color shift TTFs 56

Table 5-3 Parameter estimation result with maximum likelihood estimation (t_f) 60

Table 5-4 Parameter estimation result with maximum likelihood estimation (t_{fc}) 61

Table 5-5 Results of goodness-of-fit test and estimated MTTF of luminance degradation using a common shape parameter 63

Table 5-6 Results of goodness-of-fit test and estimated MTTF of color shift using a common shape parameter 64

Table 5-7 Least squares regression analysis 67

Table 5-8 Acceleration factor at six times the initial luminance intensity 68

Table 5-9 Estimated lifetime and validity check 71

Table 5-10 Least squares regression analysis 72

Table 5-11 Acceleration factor at six times the initial luminance intensity 73

Table 5-12 Estimated lifetime and validity check 75

Table 6-1 Least squares regression analysis 80

Table 6-2 The calibrated vector of the unknown variables 91

List of Figures

Figure 2-1 Simplified view of the model verification and validation process. 18

Figure 2-2 A framework for statistical model validation in the product development process 23

Figure 3-1 Comparison of pixel structure: (a) sub-pixel of a smartphone and (b) sub-pixel of a large OLED TV. 28

Figure 3-2 Defining reliability issues of OLED displays through a non-uniform temperature profile and examining the color shift phenomenon. 29

Figure 3-3 7-step MacAdam ellipse plotted on the 1931 CIE color space and the dimension description of the ellipse 32

Figure 3-4 Cross-sectional diagram of a sub-pixel (left) and a tandem OLED having two EL units (right). 33

Figure 3-5 The comparison of decay speed in each color of OLED TV. 35

Figure 3-6 The characteristics of SED curve by each parameter. 37

Figure 4-1 The display pattern of OLED panels used for the accelerated degradation testing. 42

Figure 4-2 Test results of color shift in four patterns of OLED panels. 44

Figure 4-3 Temperature deviation in the OLED panel at each ambient temperature; Position 1 corresponds to the spot in the top-left corner of the panel, while Position

36 is the spot in the bottom-right of the panel. 45

Figure 4-4 Luminance degradation test and curve fitting results..... 46

Figure 4-5 Test results of color shift in the 7th pattern of Set ID #1 at a 40°Ctemperature condition over time. 48

Figure 4-6 Test results of color coordinates in each accelerated condition. 48

Figure 4-7 Box plot of the time to failure (t_f) estimated from the SED curve. 49

Figure 4-8 Test and curve fitting result of color shift estimated from the Power curve. 51

Figure 4-9 Box plot of the time to failure (t_{fc}) estimated from the Power curve. 52

Figure 5-1 The observed lifetime data and the Weibull distribution of luminance degradation..... 54

Figure 5-2 The observed lifetime data and the Weibull distribution of color shift..... 54

Figure 5-3 Lifetime distribution plot drawn on Weibull probability paper..... 57

Figure 5-4 The value of the log-likelihood function according to the common shape parameter (β). 60

Figure 5-5 Lifetime distribution plot drawn on Weibull probability paper..... 61

Figure 5-6 Regression results of the bivariate luminance lifetime model estimated using MTTF. 67

Figure 5-7 Lifetime distribution calculated from the model and AF: (a) initial luminance intensity and (b) temperature. 68

Figure 5-8 Comparison between testing and estimated results. 71

Figure 5-9 Regression result of bivariate color shift lifetime model estimated using MTTF. 72

Figure 5-10 Lifetime distribution calculated from the model and AF: (a) initial luminance intensity and (b) temperature. 73

Figure 5-11 Comparison between testing and estimated results. 75

Figure 6-1 Test and regression results: The unfilled circle is the test result at room temperature (25℃); the solid circle is the test result at 40℃. The red line is estimated using the exponential regression model. 80

Figure 6-2 Description of finite element model for thermal analysis. 81

Figure 6-3 Resultant temperature contour of simulation. 81

Figure 6-4 The statistical calibration procedure. 86

Figure 6-5 The transformation of experimental temperature (y_i) from the predicted PDF estimated by the simulation result. 88

Figure 6-6 Calculation of area metric. 89

Figure 6-7 Initial guess and calibrated values for surface temperature at the 27th, 28th, 29th, and 31st pattern of three OLED panels under a 25℃temperature condition. . 90

Figure 6-8 Area metric and hypothesis results obtained with 84 test results in the calibration and validation domains. 91

Figure 7-1 Top view of simulation domain (left) and side view (right) 93

Figure 7-2 Simulation results: (a) Velocity of fluid domain, (b) Temperature of fluid domain, and (c) Temperature of OLED panel. 94

Figure 7-3 The comparison between the heat transfer coefficient from CFD result, and from theoretical value. 95

Figure 7-4 The estimated color shift lifetime. 96

Figure 7-5 The estimated luminance degradation from SED curve and AF by surface temperature. 97

Figure 8-1 An improved design process by enabling concurrent engineering and reliability estimation. 102

Nomenclature

ALD = accelerated testing

AF = acceleration factor

RUL = remaining useful life

LSR = least square regression

TFT = thin film transistor

TTF = time to failure

ATSC = Advanced Television System Committee

IEC = International Electrotechnical Commission

CIE = the Commission Internationale de l'Eclairage

MTTF = the mean time to failure

BET = Brunauer, Emmett and Teller

y = experimental data

u = the cumulative density corresponding to all experimental data

$F(y)$ = predictive cumulative density function

Um = area metric determined by calculating the area between the CDF of the uniform distribution and the empirical CDF of u value

α = a significant level

β = the shape parameter of the Weibull distribution

$\tilde{\beta}$ = the common shape parameter

η = the shape parameter of the Weibull distribution

ϑ = the ideal limit of luminance intensity

$\boldsymbol{\theta}$ = unknown model variable vector

$\boldsymbol{\Theta}$ = calibration parameter vector

μ = mean

σ = standard deviation

$D_i(\alpha)$ = a critical value of the area metric using the empirical probability distribution of the area metric

$l(t)$ = performance luminance model according to time (t)

$c(t)$ = performance color shift model according to time (t)

t_f = the time to failure of luminance degradation (time to 50% degradation)

t_{fc} = the time to failure of color shift

AF_{lum} = the acceleration factor of luminance degradation for initial luminance intensity

AF_{C} = the acceleration factor of color shift for initial luminance intensity

AF_{temp} = the acceleration factor for temperature

L = the likelihood function

L_{n} = the lifespan of luminance degradation under normal usage conditions

L_{Cn} = the lifespan of color shift under normal usage conditions

L_{a} = the lifespan of luminance degradation under accelerated loading conditions

L_{Ca} = the lifespan of color shift under accelerated loading conditions

I_{lumn} = the initial luminance intensity under normal usage conditions

I_{luma} = the initial luminance intensity under accelerated loading conditions

T_{n} = the temperature under normal usage conditions

T_{a} = the temperature under accelerated conditions

H_0 = the null hypothesis

H_1 = the alternative hypothesis

$\chi^2(1\text{-}\alpha; J\text{-}1)$ = the $100^{th}(1\text{-}\alpha)$ percentile of the chi-square distribution with J-1 degrees of freedom

Chapter 1. Introduction

1.1 Background and Motivation

White organic light-emitting diode (WOLED) displays have recently gained attention due to their simple fabrication process, thin structure, and display qualities that include a wide viewing angle and high contrast ratio. OLED technology has already successfully penetrated the television (TV) market, and the versatility of OLED is expected to make future design innovation in televisions more flexible and transparent. However, remaining reliability issues must be solved before OLED displays can be widely adopted. The primary issue is that OLED luminance degrades over time. This degradation not only reduces the display luminance, but also shifts its emission color. To date, reliability issues related to both luminance and color shift have been overcome by implementing a tandem structure for the emissive layer and through additional testing during the manufacturing process. In particular, a tandem structure of the emissive layer is suitable for mass production of large-sized OLED TVs because it overcomes various limitations otherwise found in mass production of OLEDs, such as sagging and misalignment of the fine metal mask [1, 2].

Numerous experimental studies have been conducted to date to assess the reliability of solid-state lighting, mostly through accelerated life testing (ALT). Prior research has also been conducted to find a relevant acceleration model that represents

the effect of operational conditions on the degradation of OLEDs. Several studies employed a single acceleration factor (AF) to build an acceleration model. However, OLED panels in real-world applications (e.g., TV sets) are subjected to a combination of AFs. Moreover, individual OLED pixels in the panel are subjected to various physical and operating uncertainties. Although numerous mature technologies that were developed for LCDs are being incorporated into OLED displays, it is still challenging to address these uncertainties in large OLED panels. Thus, to date, no statistical analysis procedures have been developed that incorporate manufacturing and operational uncertainties to accurately estimate the lifetime distribution of large OLED panels.

1.2 Overview and Significance

This research encompasses four advanced research areas necessary for estimating the nominal lifetime of OLEDs: Research Thrust 1 – design of accelerated degradation tests for OLED panels, Research Thrust 2 – development of two novel bivariate acceleration models, Research Thrust 3 – a systematic scheme to build bivariate lifetime models for OLED panels, and Research Thrust 4 – statistical model validation of a heat dissipation analysis model. The proposed statistical approach considers manufacturing and operational uncertainties throughout a likelihood-ratio-based validation method; this approach will provide guidance to quality and reliability engineers. The two proposed novel bivariate lifetime models can estimate

the exact nominal lifetime of luminance and color shift with the interaction term between the ambient temperature and the luminance intensity. The proposed models outperform existing models. Based on the empirical relationship between surface temperature and time to failure (TTF) of color shift, the reliability of color shift can be predicted at an early stage of product development through surface temperature analysis. The statistical validation procedure for heat dissipation analysis for large OLED TV sets with various uncertainties is outlined in Research Thrust 4. Thus, the research scope of this thesis is to develop technical advances in the following four research thrusts:

Research Thrust 1: Design of Accelerated Degradation Tests

Research Thrust 1 suggests an experimental setup for accelerated degradation tests to overcome the limited sample sizes of real-world applications and to consider the spatial uncertainty present in OLED panels. This research is needed, because reliability engineers and product designers of commercial manufacturers have difficulty getting enough samples for degradation tests at the early design stages of product development. Thus, the design of this experiment that considers two main acceleration factors – initial luminance intensity and ambient temperature – will provide much-needed reductions in the test period during the design phase. The display pattern in each TV set is suggested to consider the spatial temperature variation by the natural convection effect and the electrical components on the back of the OLED panel.

Research Thrust 2: A Systematic Scheme to Build Bivariate Lifetime Models for OLED Panels

Research Thrust 2 addresses the research challenge that there is presently no statistical procedure to analyze the accelerated test data of OLED panels; these panels are subject to various uncertainties and test samples of panels are not many. The procedure consists of: (1) estimation of the time to failure (TTF) using accelerated data and the proposed degradation model, (2) inference of a common shape parameter of the lifetime distribution, (3) evaluation of validity through likelihood ratio analysis, (4) prediction of the lifetime distribution of OLED panels via the proposed bivariate AF model, and (5) validation of the proposed model by comparison with observed data.

The two main statistical validity checks suggested in this study are the *likelihood ratio analysis* for checking the validity of a common shape parameter of the lifetime distribution and the *goodness-of-fitness* test for comparing the estimated lifetimes derived from the regression model and from the observed data.

Research Thrust 3: Two Bivariate Lifetime Models

Research Thrust 3 suggests two novel bivariate lifetime models to estimate the lifetime under normal usage conditions. Extensive prior research studies have focused on acceleration of OLED degradation with a single acceleration factor (AF). However, OLED panels in real-world applications (e.g., TV sets) are subjected to a

combination of AFs. The AFs for degradation of OLEDs include the operating temperature and the driving current (or initial luminance intensity).

The first novel bivariate lifetime model is proposed to analyze the lifespan testing data for OLEDs' luminance degradation. The proposed bivariate lifetime model, which includes an interaction term between the ambient temperature and the luminance intensity, outperformed existing models.

The second proposed novel bivariate lifetime model examines OLED lifetime as related to color shift; the model assumes that the acceleration factor of initial luminance intensity follows the BET (Brunauer, Emmett and Teller) theory, and that the temperature follows the Arrhenius equation.

The normal life estimated using both of these proposed bivariate lifetime models showed exact agreement with the experimental data.

Research Thrust 4: Statistical Model Validation of the Heat Dissipation Analysis Model

Following the development of Research Thrust 3 for estimation of the OLED lifetime resulting from color shift, Research Thrust 4 is designed to estimate color shift reliability through surface temperature data that is acquired from a computational heat dissipation model with high fidelity throughout a model validation framework. Most OLED TV manufacturers continuously try to reduce the

product design period and manufacturing cost. Thus, manufacturers have focused on reducing the time needed for analyzing OLED reliability. The key to success in this effort is to verify how quickly the various reliability criteria of the product are met when innovative materials and manufacturing processes are applied.

The proposed thermal analysis model that was statistically calibrated and validated out of the calibration domain is expected to allow thermal designers and quality engineers to estimate the display quality through a verification and validation (V&V) framework. Additionally, a regression model in which the lifetime of color shift is related to the surface temperature of the OLED panel will help thermal engineers estimate the lifetime as it relates to color shift in the early stages of product development.

1.3 Thesis Layout

The thesis is organized as follows. Chapter 2 reviews the current state of knowledge related to OLED degradation models and model verification and validation. Chapter 3 describes a review of chromaticity and degradation mechanisms of OLEDs with consideration of luminance and color shift. Chapter 4 presents an experimental method for accelerated life testing and the definition of the time to failure for luminance degradation and color shift. Chapter 5 presents a proposed bivariate lifetime model for OLEDs. In addition, we show that the lifespan

distribution of OLEDs statistically follows the Weibull distribution; we also estimate the common shape parameter. Chapter 6 presents the statistical model validation framework for a computational model that can estimate the surface temperature of OLEDs, and the related process of statistical model calibration. Finally, Chapter 7 summarizes the contribution of this research and provides insight on future work.

Chapter 2. Literature Review

This chapter provides a review of the state-of-art knowledge for OLED reliability that is within the scope of the research described in this thesis, including: (1) accelerated testing, (2) luminance degradation models for OLEDs, (3) color shift of OLED, and (4) verification and validation methodologies.

2.1 Accelerated Testing

Numerous experimental studies have been conducted to date to assess the reliability of solid-state lighting, mostly through accelerated testing (ALT) [3-5]. Many researchers have studied traditional destructive life testing, which records failure data [6, 7]. The goal of accelerated testing is to estimate the nominal lifetime of OLEDs when subjected to normal usage conditions that would be expected in service [8]. The steps for accelerated testing include (1) testing samples under accelerated loading conditions, (2) estimating the lifetime distribution and determining an acceleration factor (AF), and (3) calculating lifetime distributions under normal usage conditions. The second step is regarded as the most critical to enable prediction of an accurate lifetime distribution [9, 10].

Previously, both parametric and non-parametric approaches have been used to estimate lifetime distributions. The parametric approach involves a selection process for choosing a set of distribution parameters that gives the largest correlation for the

given experimental data. For example, Zhang *et al*. [7, 11] showed that the lifespan of a white OLED under current loading conditions meets lognormal and Weibull distributions. Wang *et al*. [12] presented a general procedure for the parametric approach to lifespan prediction. The non-parametric approach involves estimating the lifetime without relying on a closed-form expression for the statistical distributions. The non-parametric approach can be implemented for any type of experimental data. However, one of the challenges of this approach is to calculate second-order derivatives of the performance degradation equation. For example, Park [13] compared the performance of conventional lifetime distribution-based approaches (such as Weibull and lognormal distributions) with that of the non-parametric method. Park's work showed that the non-parametric method for OLED degradation determination gives a comparable result to parametric methods, when the proper lifetime distribution is unknown. In contrast, the parametric approach provides more accurate estimates in terms of the percentile lifetime.

As the expected lifetime of OLEDs and LEDs lengthens due to high-fidelity materials and the compensation algorithm, it has become prohibitively expensive for quality engineers to estimate lifetime via traditional destructive life testing. In order to overcome this challenge, researchers have sought ways to predict the remaining useful life (RUL) of displays without a significant number of samples and at earlier testing times. Both deterministic and statistical approaches have been used to estimate RUL. Deterministic approaches involve the least square regression (LSR)

for parameter estimation in a lumen degradation model. Park [13] presented a bi-exponential model and Zhang et al. [4] utilized a stretched decay model to describe the relationship between an OLED's luminance degradation and time.

When degradation data are fragmented or sparsely observed, nonparametric degradation models may be used because one cannot clearly trace how a degradation path progresses over time from incomplete observations [14]. Two common classes of stochastic process are the gamma [15-17] and the Weiner [18, 19] processes. Wang and Xu [20] showed that the inverse gamma Gaussian (IG) process has been reported as an attractive and flexible model for degradation modeling. Chen [21] justified the physical meaning of the IG process by exploring the inherent relations between the IG process and the compound Poisson process. By linking the Weiner process, he investigated different options to incorporate random effects in the IG process model.

The LSR method has many weaknesses in terms of guaranteeing prediction accuracy, because it does not consider the uncertainties. To improve the accuracy of lifetime prediction and reduce the test time, the technique of prognostics and health management (PHM) has been adopted in light displays, such as plasma display panels (PDPs), and organic light emitting displays (OLEDs).

In general, prognostic approaches can be categorized into model-based approaches [22-24], data-driven approaches [25, 26], and hybrid approaches [27].

The application of general model-based approaches relies on the understanding of system physics-of-failure and underlying system degradation models. As high-risk engineered systems generally consist of multiple components with multiple failure modes, for complex systems, it is almost impossible to understand all potential physics-of-failures and their interactions. Fan et al. [28, 29] presented a nonlinear, filter-based prognostic approach to improve the prediction accuracy of luminance for high-power, white light emitting diodes based on short-term observed data. In particular, a reasonable initialization process for the parameters based on historical databases or calibration testing is needed to guarantee the advantages of the particle filter (PF) method.

With the advance of modern sensor systems, data storage and processing technologies, data-driven approaches for system health prognostics have become popular; these are mainly based on massive sensory data with reduced requirements for knowing inherent system failure mechanisms. Data-driven prognostic approaches generally require sensory data fusion and feature extraction, statistical pattern recognition, and for life prediction, the interpolation, extrapolation, or machine learning. Due to the long testing times and expensive test samples, there are few examples of data-driven prognostics approaches.

2.2 Luminance Degradation Model for OLEDs

Extensive prior studies have been conducted to find a relevant acceleration model that represents the effect of operational loading conditions on the degradation of OLEDs. First, it has been shown that the acceleration of degradation due to luminance intensity is governed by the inverse power relationship [11]. Second, the acceleration of degradation due to temperature is dictated by the Arrhenius equation. It was shown that localized Joule heating significantly reduces the operational lifetime of OLEDs [30]. Several studies in the literature [7, 11, 13, 31] employed a single AF to build an acceleration model. However, OLED panels in real-world applications (e.g., TV sets) are subjected to a combination of AFs. It is commonly observed that a different amount of heat is dissipated by conduction and natural convection form individual electric components. Moreover, the luminance intensity produced by the driving current nonlinearly increases with respect to the operating temperature [32]. To the best of our knowledge, no study to date has incorporated multiple AFs.

In real-world applications, individual OLED pixels in a panel are subjected to various physical and operating uncertainties [33-35]. For example, in the process of plasma-enhanced chemical vapor deposition, the TFT in an OLED panel does not crystallize in a perfectly uniform manner. Thus, the current consumed by each individual pixel of the TFT varies [36]. Numerous studies have suggested advanced TFT fabrication processes and developed new compensation methods for

minimizing this uncertainty; however, it still remains as an issue [36, 37]. Another example of uncertainty is the large spatial deviation in temperature that occurs due to local heat sources and natural convection in the slim design of a large display [34, 38].

In general, the decrease of OLED luminance over time proceeds through three independent and visually distinct degradation modes: (1) dark-spot degradation, (2) catastrophic failure, and (3) intrinsic degradation.

While the first two modes of degradation can be effectively controlled by means of proper device encapsulation and adequate control over device fabrication conditions, the intrinsic degradation mode has been far more challenging and continues to be an issue for OLED commercialization.

One widespread approach is to describe the performance degradation of OLEDs' luminance degradation over time using a combination of exponential decays, commonly using two terms. The first term accounts for the rapid initial decay, the second term accounts for the long-term degradation [39]. Howard [40] & Ishii [41, 42] reported that a far better way is to use a stretched exponential decay (SED).

Summary and Discussion

Although numerous mature technologies that were developed for LCDs are being incorporated into OLED displays [5, 43, 44], it is still challenging to address these

uncertainties in large OLED panels. Thus, to date, no statistical analysis procedures have been developed that incorporate manufacturing and operational uncertainties to accurately estimate the lifetime distribution of large OLED panels.

2.3 Color Shift of OLEDs

Besides luminance degradation, another reliability issue of the tandem OLED structure is color shift over operating time. Digital TV manufacturers strive to meet Advanced Television Systems Committee (ATSC) standards. ATSC is an international, non-profit organization that develops voluntary standards for digital television. Also, IEC 62341 [45] describes the measuring methods for visual quality and ambient performance of displays. To date, there is little practical guidance on reliability criteria based on color shift in display devices. Sugimoto et al [46] suggested an accelerated method for evaluating color shift of white OLED panels. Chen et al. [47] proposed an evaluation method for OLEDs as light sources. However, no standards or research have yet suggested criteria for color shift over time due to the lack of information about the mechanism of color shift and test results for large-sized displays. Accordingly, here, we suggest a novel bivariate lifetime model for color shift in OLED displays.

In real-world applications, individual OLED pixels in a panel are subjected to various manufacturing and operating uncertainties. In particular, the large spatial

deviation in temperature due to local heat sources and natural convection in the slim design of a large display accelerates reliability issues, such as color shift and image sticking [48].

Because reliability issues are related to thermal conditions, many researchers have used simple thermal models to study estimation methods for thermal behavior in the OLED structure during transient current conditions [35, 49]. Pang suggested an indirect method to accurately calculate the lifetime of large-sized OLED panels, without testing the panels directly [3]. Slawinski et al. characterized the electrothermal behavior of large-area OLEDs by employing finite-element simulation and considering natural convection with vertical position [33]. Despite these efforts, it is still challenging to exactly estimate junction temperature in large-sized commercial OLED displays due to their complicated structure and individual electric components.

Summary and Discussion

This study aims to develop a lifetime model for color shift that (1) accurately predicts the lifetime of large OLED panels under actual usage conditions, and (2) estimates color shift reliability through surface temperature data that is acquired from a computational heat dissipation model with high fidelity throughout a model validation framework.

2.4 Verification and Validation Methodology

As the role of computational models has increased, the accuracy of the computational results has become important to analysts who make decisions based on these predicted results. Among various works on model verification and validation (V&V), survey articles have been introduced by various engineering groups, including the American Institute of Aeronautics and Astronautics (AIAA) [50], the American Society of Mechanical Engineers (ASME) [51], the Department of Energy Laboratories (Sandia [52], Loss Alamos [53], and Lawrence Livermore [54]), and Institute for Computational Engineering and Sciences (ICES) [55]; these articles explain the state-of-the-art concepts, terminology, processes, and model techniques in detail. In these works, verification is briefly defined as the assessment of the accuracy of a computational model implementation; validation is defined as the assessment of the accuracy of computational results by comparison with experimental data [52]. The important concepts for model V&V addressed in those references are summarized below.

Model Verification

In the ASME guidelines, model verification is defined as "the purpose of determining that a computational model accurately represents the underlying mathematical model and its solution." Verification deals with the relationship between a mathematical model and its programmed implementation in the code (the

computational model). Verification is mainly conducted by comparing numerical solutions of the computational model to highly accurate benchmarking solutions. The use of benchmarking solutions in verification is called "testing" in the software engineering community [56]. Verification generally is divided into two activities: (1) code verification and (2) calculation verification [52, 57]. The major goal of code verification is to confirm that the mathematical model (computer software) is working as intended. Calculation verification is performed to evaluate the accuracy of the discrete solution of the mathematical model by estimating the numerical errors that arise due to discretization approximations. Insufficient spatial or temporal discretization, insufficient convergence tolerance, incorrect input options, and/or finite precision arithmetic can be identified using calculation verification. It is relatively popular to perform code-to-code comparisons as a means of calculation verification in the absence of sufficient verification evidence from other sources.

Model Validation

As shown in Figure 2-1, model validation deals with the relationship between the computational results from a computational model and reality, i.e., the experimental results. Model validation is defined as the process of determining the degree to which a model is an accurate representation of the real world from the perspective of the intended uses of the model [51, 52]. The phrase "process of determining" emphasizes

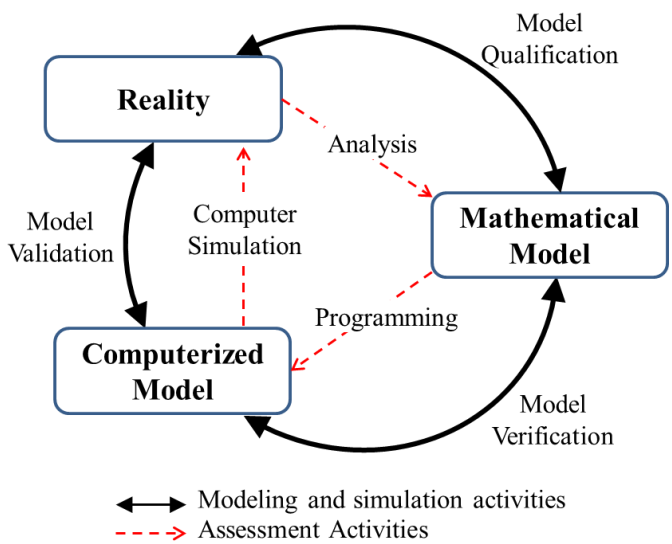

Figure 2-1 Simplified view of the model verification and validation process.

that model validation is an ongoing activity that concludes only when acceptable agreement is achieved between experiment and simulation. The phrase “degree to which” emphasizes that the simulation and the experimental results are uncertain. Finally, the phrase “intended uses of the model” emphasizes that the validity of a model is defined over the domain of model form, input variables, and predictive responses. In order to quantitatively determine the degree of validity, a comparison between the experimental and computational results has to be performed using a validity check metric; several metrics are available. Oberkampf et al. [58] developed a validity check metric based on the concept of statistical confidence intervals. Ferson et al. [59] used the integrated area between the cumulative distribution

functions (CDFs) of experimental and computational results as a validation measure. Rebba et al. [60] used the distance metric based on the Anderson-Darling statistics.

Model Calibration

While model validation primarily assesses the confidence of computational results, model calibration is different in that it is a process of maximizing the agreement of predicted results with respect to a set of experimental data through the adjustment of a set of physical input variables. In the computational engineering field, model validation sometimes includes a model calibration activity, which involves the estimation or optimization of model input variables using experimental data from a system [61, 62]. For successful calibration, the distinction between the calibration variable and the tuning variable must be clearly understood. The calibration variables have a physically interpretable meaning; however, the tuning variable may be notional and may have little or no meaning in the physical system.

To improve the predictive capability of a computational model, model calibration techniques have been developed in recent years. Model calibration adjusts a set of unknown model input variables associated with a computational model so that the agreement is maximized between the predicted (or simulated) and observed (or experimental) responses (or outputs). In a deterministic sense, model calibration is thought of as the adjustment of a few model input variables to minimize the discrepancy between the predicted and observed results. However, the deterministic

approach is not appropriate because various uncertainties exist in the material properties, loading condition, boundary condition, etc. Statistical model calibration, on the other hand, means refining the probability distributions of unknown input variables through comparison of the predicted and observed outputs [63]. Current statistical model calibration is mainly based on methods of moments [64], Bayesian statistics [65-67], and maximum likelihood estimation [68]. Statistical model calibration with Bayesian statics mainly focuses on the surrogate model (also called the metamodel [69]), which replaces expensive computational models of engineered systems. In computational engineering, it is common for computational models to take hours or days to run. Because it is, in general, impossible to conduct enough simulation runs to thoroughly cover the entire input variable space for design purposes, surrogate models – such as polynomial function and kriging model [44] – have been developed with design of experiment techniques [70]. The drawback of simply using a fitted metamodel is that it may ignore metamodel uncertainty, i.e., the uncertainty that results from not knowing the output of the expensive computational model, except at a finite set of sampling points.

Uncertainty Propagation

Uncertainty propagation (UP) analysis is an essential part of statistical model calibration. UP analysis refers to the determination of the uncertainty in analysis results that is propagated from uncertainties in the input variables of a computational model that arise because of the inherent randomness in physical systems (material

properties, boundary condition, etc.), modeling idealizations, experimental variability, measurement inaccuracy and manufacturing tolerance. Existing UP analysis methods can be grouped into four categories: (1) the sampling method, (2) the expansion method, (3) the metamodeling method, and (4) the approximate integration method.

(1) The sampling method: The sampling method is the most comprehensive, but most expensive method, for estimating moments and the reliability of system responses. Sampling methods draw samples from the input parameter populations, evaluate the deterministic model using these samples, and then build a probability density function (PDF) of the responses. Monte Carlo Simulation (MCS) [71, 72] is the most widely used sampling method; however, MCS demands thousands of computational analyses. To relieve the computational burden, other sampling methods have been developed, such as quasi-MCS [73], important sampling [74], and directional sampling [75].

(2) The expansion method: The expansion method estimates statistical moments of system responses using a small perturbation to simulate input uncertainty. Expansion methods include Taylor expansion [76], the perturbation method [77], the Neumann expansion method [78], etc. Overall, all expansion methods can become computationally inefficient or inaccurate when the amount or the degree of input uncertainty is high. Moreover, since it requires high-order partial sensitivities of system responses, it may not be practical for large-scale engineering applications.

(3) The metamodeling method: There currently exist a number of metamodeling techniques, such as polynomial response surface model (PRSM), multivariate adaptive regression spline (MARS), radial basis function (RBF), kriging, neural networks, and support vector regression (SVR). Each technique has its own fitting method. For example, PRSM is usually fitted with the (moving) least squares method [79]; the kriging method is fitted with a search for the best linear unbiased predictor [79]. In general, kriging models can produce accurate results for nonlinear problems; however, they are difficult to obtain and use because a global optimization process must be applied to identify the maximum likelihood estimators [80]. Although neural networks are able to accurately approximate very complex models, they have two disadvantages: (1) they are a "black box" approach, and (2) the have a computationally expensive training process [81].

(4) The approximate integration method: The approximate integration method is a direct approach to estimate the probability density function (PDF) or statistical moments through numerical integration. Numerical integration can be done in the input uncertainty domain [82] or in the output uncertainty domain [83]. In the univariate dimension reduction method, this method uses an additive decomposition of the responses that simplifies one multi-dimensional integration to multiple one-dimensional integrations. Generally, the method can provide accurate lower moment of system responses, such as mean. However, it may produce a relatively large error for second-order or higher moments of nonlinear system responses. In the general

dimension reduction method [84], the theoretical error of the univariate dimension reduction method can be reduced by considering multi-dimensional integrations. However, the computational effort increases exponentially to achieve this error reduction.

A Hierarchical Framework for Statistical Model Validation

Increased customer expectations have resulted in new product developments at an ever-increasing pace. The product development process is traditionally conceived of as a cost-intensive and time-consuming process because it requires repeated product prototyping and testing to improve product performance and reliability. Jung et al. suggested a framework of model validation and virtual product testing [61, 85],

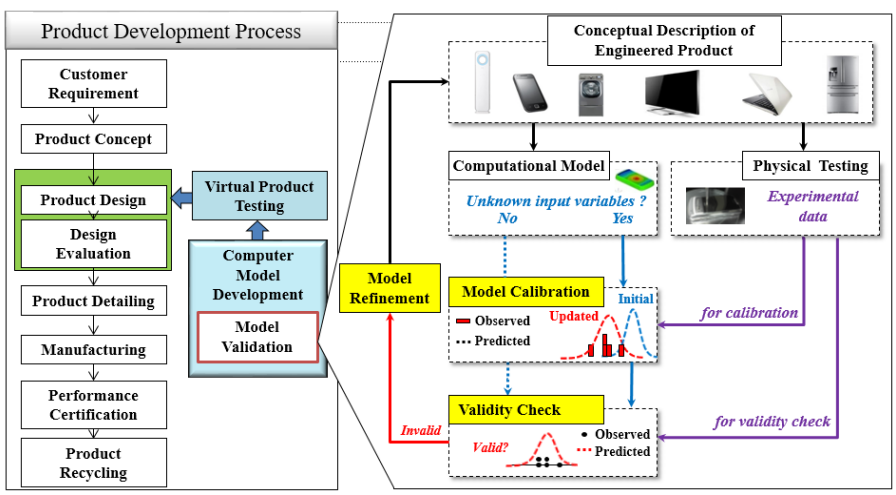

Figure 2-2 A framework for statistical model validation in the product development process.

as shown in Figure 2-2. They proposed a framework of virtual testing based on statistical inference for new product development comprised of three successive steps: (1) statistical model calibration, (2) a hypothesis test for validity checking and (3) virtual qualification. Statistical model calibration first improves the predictive capability of a computational model in a calibration domain. Next, a hypothesis test is performed using limited observed data to see if the calibrated model is sufficiently productive for virtual testing of a new product design. An area metric and the u-pooling method [59] are employed for the hypothesis test to measure the degree of mismatch between predicted and observed results.

The u-pooling method is beneficial because it allows integration of all experimental data from various experimental settings (e.g., environmental temperature, loading) into a single aggregate metric. In the u-pooling method, the cumulative density, u_i, should be first obtained by transforming every experimental datum (y_i) according to its corresponding predictive CDF (F_{yi}) of the calibrated model as:

$$u_i = F_{yi}(y_i) \tag{2.1}$$

where i is the number of experimental data. Under the assumption that the experimental data, y_i, truly come from the mother distribution (or mother function), the u_i values corresponding to all experimental data will follow a uniform distribution [0.1]. The CDF of the uniform distribution (F_{uni}) indicates the line of

perfect agreement between the experimental data and perfect results of the calibrated model. Therefore, any mismatch between the dispersion of experimental data and the predicted results can be determined by calculating the area (i.e., the area metric (U_m)) between the CDF of the uniform distribution (F_{uni}) and the empirical CDF of u_i values (F_u) as:

$$U_m = area(F_u, F_{\text{uni}}) = \int_0^1 |F_u(u) - F_{\text{uni}}(u)| du, \ 0 < u < 1, \ 0 < U_m < 0.5 \quad (2.2)$$

If experimental data are comprehensively collected for the validity check, there is no sampling uncertainty in the U_m and it is definite that the null hypothesis can be rejected unless the U_m is zero. In real-world settings, experimental data are limited, thus, the U_m has uncertainty, although the mother distributions of predicted and experimental results are identical (i.e., the model is valid). The uncertainty in our metric is characterized using a virtual sampling technique with the following three steps.

Step 1: Assume that the mother distributions of the predicted and experimental results are identical (i.e., the model well-represents the physical responses, in other words, model is valid).

Step 2: The *i* number of experimental data are virtually sampled from the mother distribution, and the *u* values and the corresponding U_m are calculated using Equation (2.2).

Step 3: Step 2 is repeated several thousand times and a statistical distribution (i.e., PDF) of the U_m ($f_{u,i}$) is constructed with U_m values using a Pearson system [86]. A Pearson system can appropriately represent the uncertainty in U_m.

The hypothesis test uses the PDF of the area metric ($f_{u,i}$). Because the $f_{u,i}$ indicates plausible values of U_m in case the mother distributions of the predicted and experimental results are identical, an upper-tailed test can be employed after deciding a rejection region as:

$$U_m > D_i(\alpha) \tag{2.3}$$

where $D_i(\alpha)$ indicates a critical value of the area metric; α is a significance level. The null hypothesis will be rejected if and only if U_m falls in the rejection region. In the absence of such evidence, H_0 should not be rejected, because it is still plausible.

Summary and Discussion

Most OLED TV manufacturers continuously work to reduce the product design period and manufacturing cost. In support of this goal, manufacturers have focused on reducing the time needed for analyzing OLED reliability. The key to success in this effort is to verify how quickly the various reliability criteria of the product are met when innovative materials and manufacturing processes are applied.

Considerable attention has been paid to developing verification and validation (V&V) methodologies that improve and assess the predictive capability of computational models [85]. Statistical model calibration requires uncertainty propagation (UP) analysis, such as the eigenvector dimension reduction (EDR) method, to develop the statistical responses of a computational model [87].

Chapter 3. OLED Degradation

The invention of organic light-emitting diodes (OLEDs) has opened a way toward next-generation informational displays and solid-state lighting sources. Currently, small-sized, full-color OLED displays are in mass production on Gen. 5.5 glass for portable electronic devices. Three colors of RGB sub-pixels can be patterned through the evaporation process through fine patterns of sub-pixel size that are formed on the fine metal mask (FMM) [88, 89]. However, this method is not suitable for large-sized OLED displays due to the defects and color mixing that are caused by sagging and misalignment of the FMM. Therefore, large-sized displays (e.g., TV applications) require a new color patterning method in order to avoid these problems. For large-sized OLED TV and lighting, white organic light-emitting diode (WOLED) technology has been developed [90-93]. Figure 3-1 shows the pixel structure of

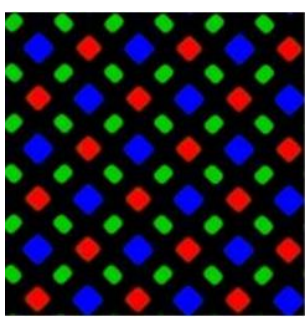

(a) RGB pixel structure of a smartphone

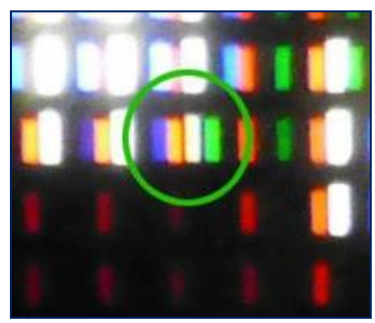

(b) WRGB pixel structure

Figure 3-1 Comparison of pixel structure: (a) sub-pixel of a smartphone and (b) sub-pixel of a large OLED TV.

small-sized and large-sized displays. WOLED overcomes various limitations otherwise found in the mass production of OLEDs, such as sagging and misalignment of the FMM. Therefore, WOLED has great potential for mass-market products.

OLED has many merits, such as its simple fabrication process, thin structure, and display qualities that include a wide viewing angle and high contrast ratio; however, there remain some challenges to overcome with this technology. The primary issue is that OLED luminance degrades over time. This degradation not only reduces the display luminance, but also shifts its emission color. In addition, the degradation rate is accelerated by temperature.

As shown in Figure 3-2, it is commonly observed that a different amount of heat is dissipated by conduction and natural convection from individual electric

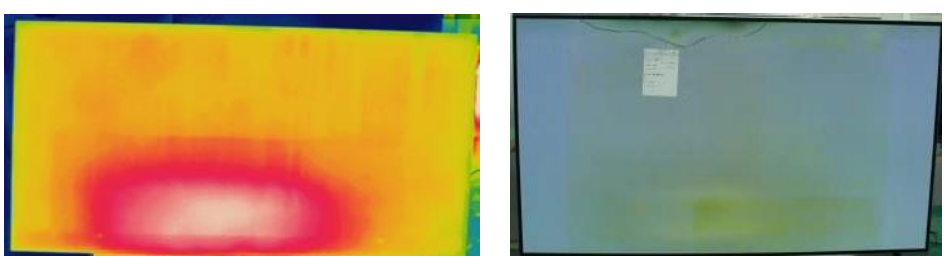

(a) The measured temperature results (b) Color shift results after accelerated test

Figure 3-2 Defining reliability issues of OLED displays through a non-uniform temperature profile and examining the color shift phenomenon.

components. Different thermal conditions cause different accelerating conditions. Eventually, this affects both luminance lifetime and color shift.

3.1 Chromaticity and the Definition of Color Shift Lifetime

Color is the brain's reaction to a specific visual stimulus. Because the eye's retina samples color using only three broad bands, humans are limited in their ability to discriminate different spectral power intensities of visible electro-magnetic radiation. The signals from these color-sensitive cells are combined in the brain to give several different sensations of color. Color shift is defined as the change in chromaticity of a light source with respect to the chromaticity at the beginning of the device's lifetime. Color shift is typically measured as Δxy or as $\Delta u'v'$ in the Commission Internationale de l'Eclairage (CIE) color coordinate systems. The chromaticity coordinates of a source provide a numerical representation of the color of the light. The three common chromaticity diagrams are the CIE 1931 (x, y), the CIE 1960 (u, v), and the CIE 1976 (u', v'). Every color is represented by unique (x, y) coordinates. The chromaticity coordinates, x, y, and z, are the ratio of X, Y, and Z coordinates of the light to the sum of the three stimulus values. It is necessary only to consider the quantity of two of the reference stimuli in order to define a color, because the three quantities (x, y, z) always sum to 1. Thus, the (x, y) coordinates are commonly used to represent a color.

The MacAdam ellipse provides a guideline as to how accurate the average person's color vision is, and how good a person is at distinguishing between similar colors [94]. The original ellipses are very small, thus, they are not typically published this way. Instead, most of the time, MacAdam ellipses are scaled up to a large size, perhaps 7× or 10× the original. In particular, a 7-step scale up is standard for color consistency used to describe compact fluorescent lamps (CFLs) and in ANSI/NEMI/ANSLG C78.3777-2008 American National Standards for Specification for the Chromaticity of Solid State Lighting (SSL) Products [95, 96]. Figure 3-3 shows the ellipses scaled up 7-steps. Because the initial white color coordinate in this study is located in the 13th ellipse, with a white color coordinate, a failure of color shift is defined as when the amount of color shift (Δxy) is greater than the distance of the major axis of the 13th ellipse of a 7-step MacAdam ellipse. A detailed dimensional description of the 13th 1-step MacAdam ellipse is described in Table 3-1. Accordingly, the time to failure of color shift (TTF, t_{f_c}) is defined as the time when the accumulated color shift (Δxy) from the initial time reaches 0.0322 ($= 7 \times 2a$).

3.2 Degradation Mechanism

A cross-sectional view of an OLED device is illustrated in Figure 3-4. Typically, an OLED panel in a large TV is composed of two structures: (1) a light-emitting

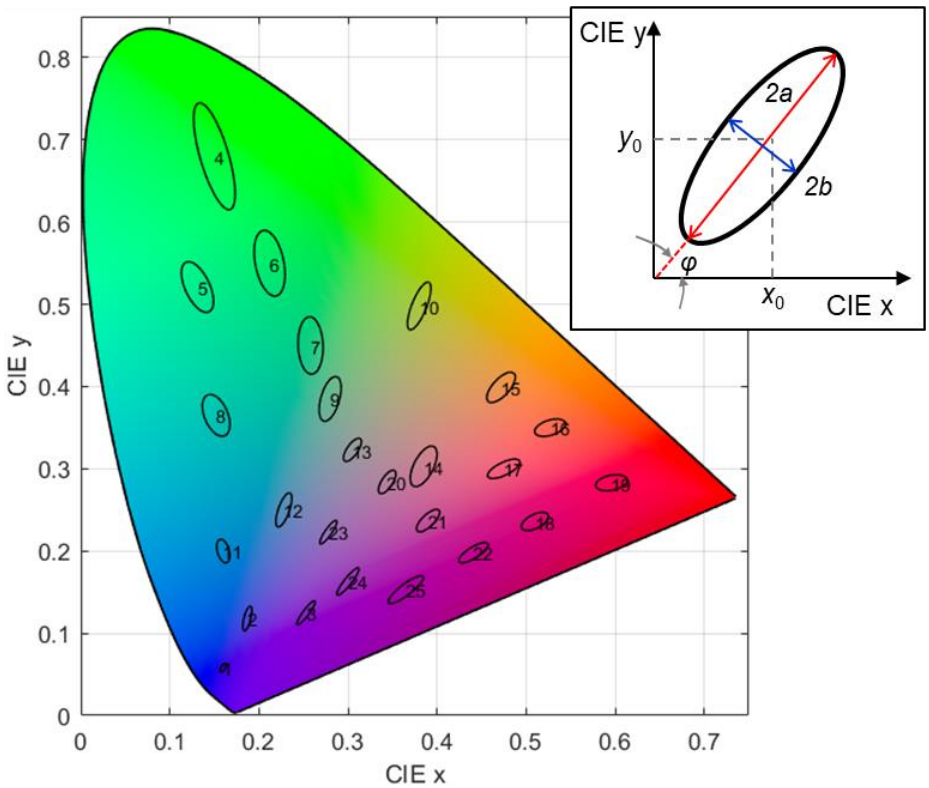

Figure 3-3 7-step MacAdam ellipse plotted on the 1931 CIE color space and the dimension description of the ellipse.

Table 3-1 13th MacAdam ellipse parameters

Center of ellipse		Ellipse parameter		
x_0	y_0	a	b	φ
0.305	0.323	2.30E-03	9.00E-04	58

layer between two sandwiched electrodes and (2) a TFT backplane [97, 98]. The TFT controls the amount of current flow by adjusting the voltage potential in the gate of the TFT. If a critical amount of current flows through the electrode of the

organic layer, it generates light while it dissipates heat. The threshold voltage of the TFT is the minimum gate-to-source voltage gap required to create a conducting path. The conducting path is then used to deliver the driving current to the light-emitting layer. Tandem OLEDs have more than one electroluminance (EL) unit connected electrically in series, with intermediate connectors within each device [2, 99].

3.2.1 Luminance Degradation Mechanism

Degradation of the light-emitting layer can be attributed to both intrinsic and extrinsic causes. Extrinsic degradation is caused by contamination and/or humidity during the fabrication process. Intrinsic degradation arises due to the electrochemical degradation that occurs in the material during the application of electric excitation; this leads to the formation of charge trapping and excited-state quenching defects

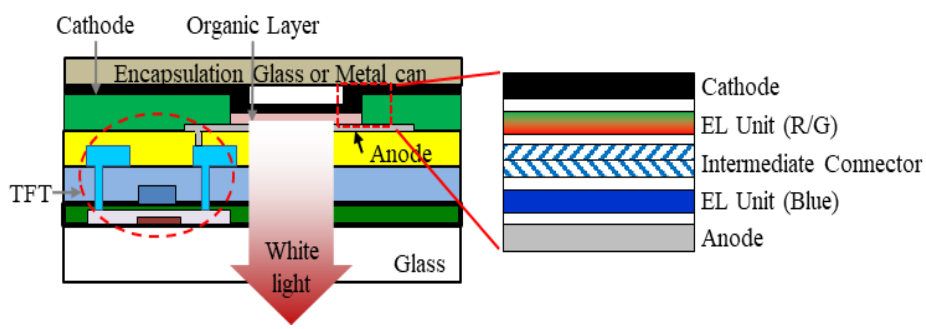

Figure 3-4 Cross-sectional diagram of a sub-pixel (left) and a tandem OLED having two EL units (right).

[100]. While extrinsic degradation can be effectively controlled through proper device encapsulation and adequate fabrication process control, intrinsic degradation is more challenging. Thus, intrinsic degradation continues to be a problematic issue that prevents widespread OLED commercialization.

As OLEDs degrade, the threshold voltage shifts over time under the elevated temperature conditions [101]. As a result, the luminance of OLEDs is also gradually reduced over time. It should be noted that the degradation of the two components – the light-emitting layer and the TFT backplane – is correlated. Thus, both failure mechanisms should be considered together for accurate OLED degradation modeling.

3.2.2 Color Shift Mechanism

White color is affected by the luminance balance between each EL unit. The main mechanism of color shift arises because the lifetime of the blue stack is shorter than that of the others [102]. Therefore, the performance degradation of color shift is not fully expressed by examining only the luminance balance between the two components. OLED TVs used in this study have the tandem WOLED structure which is composed with red/green and blue stack [99]. Therefore, white color coordinate of OLED panels shifts warm white on aging because the luminance of blue is lower than that of R/G emission.

Tandem OLEDs are OLEDs that have more than one electroluminescence unit (EL) connected electrically in series, with unique intermediate connectors within the device [2, 46]. A tandem OLED has several advantages over conventional ones [2, 103, 104]: (1) the luminance efficiency of the tandem OLED is increased linearly with the number of EL units in the device, (2) the power efficiency of a tandem OLED is also increased with the number of EL units in the device, (3) the operational lifetime of a tandem OLED is dramatically increased.

Figure 3-5 shows the decay speed of red, green, and blue color which were measured in each color pattern of OLED panels. The luminance of blue color was degraded faster than that of other color. The triangle marks (△) is the relative luminance in blue color pattern, the rectangular marks (□) in green color pattern, and diamond marks (◇) in red color pattern. The detailed experimental method will be in section 4.1.

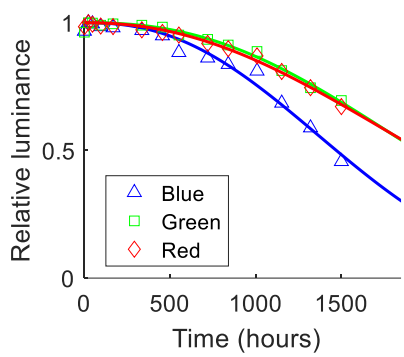

Figure 3-5 The comparison of decay speed in each color of OLED TV.

3.3 Performance Degradation Models

3.3.1 Performance Degradation Model

Several functional forms are used to describe the performance degradation of OLEDs. The double-exponential model was derived by incorporating energy transfer rates between the lowest unoccupied molecular orbit and the highest occupied molecular orbit [39]. Specifically:

$$l(t) = b_1 e^{-\alpha_1 t} + b_2 e^{-\alpha_2 t} \tag{3.1}$$

where b_1 and b_2 are the constants determined by the initial conditions; α_1 is the parameter that presents the initial decay; and α_2 is the parameter that indicates the long-term degradation according to time (t).

The stretched exponential decay (SED) model is defined as:

$$l(t) = \exp\left[-\left(\frac{t}{\tau_0}\right)^{\gamma}\right] \tag{3.2}$$

where τ_0 is the characteristic time by which the performance degrades to 63.2% of the initial performance; γ is the parameter that characterizes the degradation rate.

The SED model is useful to fit the lifetime of the OLED to the failure of the light-emitting layer of the OLEDs [105]. For example, Zhang et al. [4] tested OLEDs

under different stress conditions and fit the degradation data to an exponential function.

Degradation is largely a result of the evolution of nonemissive regions, or dark spots, which increase in both size and number with time [106, 107]. This is consistent with an increase in device resistance due to a loss of working device area. Fery [105] showed for the first time that the annihilation of the emissive centers (ECs) is the main mechanism responsible for the OLED degradation. This single mechanism is sufficient to account for both the initial rapid decay, as well as for the long term degradation. It was demonstrated that the numerical solution, which formulates the number of damaged EC at time *t* as function of total emissive centers, can be well fitted by using Equation (3.2) [108].

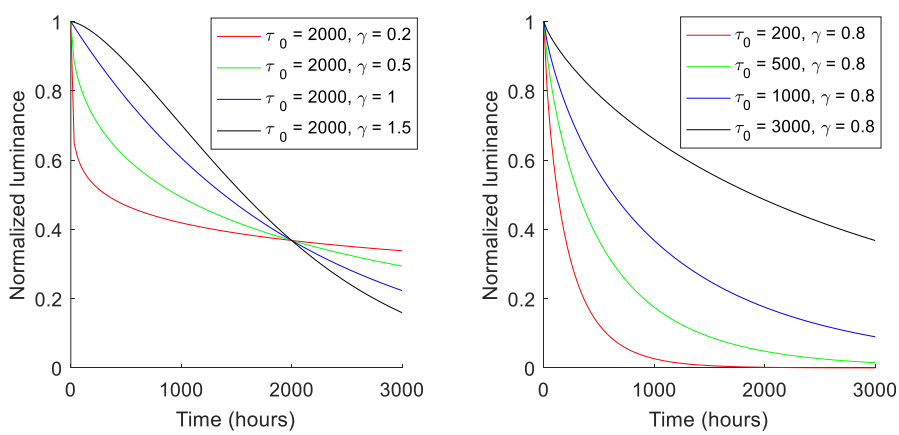

(a) By the change of degradation rate (b) By the characteristic time

Figure 3-6 The characteristics of SED curve by each parameter.

Figure 3-6 shows well the characterization of SED curve. The degradation rate, γ, expresses the initial decay characteristics, and the characteristic time, τ_0, represents 63.2% of the initial performance; each curve with same the characteristic time passes through same point as shown in Figure 3-6(a).

3.3.2 Performance Color Shift Model

As discussed earlier, a performance color shift model for OLEDs has not previously been studied. We suggest a new empirical performance model for color shift below:

$$c(t) = \varphi_1 \cdot t^{\varphi_2} \tag{3.3}$$

where φ_1 and φ_2 are the parameters that present the performance color shift degradation according to time (t). The accuracy of the proposed model is addressed in section 5.2.2.

3.4 Acceleration Model

As discussed earlier, the AFs for degradation of OLEDs include the operating temperature and the driving current (or initial luminance intensity) [109, 110]. First,

the AF for initial luminance intensity has an inverse power relationship [3, 4, 31]. The acceleration factor (AF_{lum}) for initial luminance intensity between the usage condition and the stress level is expressed by:

$$AF_{\mathrm{lum}} = \frac{L_{\mathrm{n}}}{L_{\mathrm{a}}} = \left(\frac{I_{\mathrm{lum_n}}}{I_{\mathrm{lum_a}}}\right)^{-B} \tag{3.4}$$

where L_{n} and I_{lumn} are the lifespan and the initial luminance intensity under normal usage conditions, respectively; and L_{a} and I_{luma} are the lifetime and initial luminance intensity under accelerated loading conditions, respectively.

The luminance degradation rate of each EL affects the color shift due to the structure of tandem OLEDs. Here, we propose that the acceleration factor for initial luminance intensity follows the BET (Brunauer, Emmett and Teller) equation for corrosion arising from moisture in plastic packaged electronics [111].

The acceleration factor (AF_C) for initial luminance intensity between the usage condition and the stress level is expressed by:

$$AF_{\mathrm{C}} = \frac{L_{\mathrm{Cn}}}{L_{\mathrm{Ca}}} = \left[\frac{I_{\mathrm{lum_n}}}{I_{\mathrm{lum_a}}} \cdot \left(\frac{\vartheta - I_{\mathrm{lum_a}}}{\vartheta - I_{\mathrm{lum_n}}}\right)\right]^{B} \tag{3.5}$$

where Lc_{n} and I_{lumn} are the lifespan for color shift and the initial luminance intensity under normal usage conditions, respectively; Lc_{a} and I_{luma} are the life and initial luminance intensity under accelerated loading conditions, respectively; and ϑ is the

ideal limit of the luminance intensity. In this study, ϑ was set as 11. Equation (3.5) displays a singularity as I_{lumn} and I_{luma} reaches ϑ, which is dependent on OLED characteristics. This means that the acceleration factor has singularity when the OLED turns off (I_{luma}=0) or when the OLED is set to 11 times the initial luminance.

Another acceleration factor for temperature (AF_{temp}) is expressed by [3]:

$$AF_{\text{temp}} = \exp\left[\frac{E}{k}\cdot\left(\frac{1}{T_n}-\frac{1}{T_a}\right)\right] \tag{3.6}$$

where E is the activation energy; k is the Boltzmann constant (=8.62×10^{-5}); T_{n} is the temperature under a nominal loading condition; and T_{a} is the temperature under an accelerated loading condition. It is worth noting that the acceleration models for OLEDs in previous studies employed only a single AF.

However, some accelerated tests involve more than one accelerating stress or an accelerating stress and other engineering variables. For example, many accelerated life tests of epoxy packaging for electronics employ high temperature and humidity; 85°C and 85% relative humidity (RH) are common test conditions. Peck [112] proposed such testing and proposed an Eyring relationship for lifetime, as defined below:

$$MTTF = A\cdot(RH)^{-B}\cdot e^{\left(\frac{C}{kT}\right)} \tag{3.7}$$

Intel [113] used another Eyring relationship:

$$MTTF = A \cdot e^{(-B \cdot RH)} \cdot e^{\left(\frac{C}{kT}\right)} \quad (3.8)$$

where A, B, and C are the model parameters; k is the Boltzmann constant (=8.62×10^{-5})

The Eyring equation is an equation used in chemical kinetics to describe the variance of the rate of a chemical reaction with temperature. Some semiconductor engineers implemented the Eyring equation in the accelerated life testing at multivariable condition [113, 114].

Chapter 4. Acceleration Degradation Testing (ADT) for OLEDs

4.1 Experimental Setup

Three OLED panels with the size of 1920 by 1080 pixels (See Figure 4-1) were used for a degradation test at room temperature; another three were degraded in a convection oven with a temperature of 40°C. All tested units featured a 55-inch display size, the number of pixels was 1920 by 1080, and the number of pixels in an individual pattern was 160 by 96. Four levels of luminance intensity were set for the individual OLED panels: an initial luminance intensity, and then twice, four times, and six times the initial luminance intensity (see Table 4-1). The current intensity

×1	×2	W	×2	×1	R
×4	×6	×2	×6	×4	×1
×2	W	×6	×4	×6	G
W	×6	×4	×6	×4	×1
×4	×2	×6	×4	×2	B
×1	W	×1	W	×1	×1

(a) Snapshot of test sample (b) Pattern identification

Figure 4-1 The display pattern of OLED panels used for the accelerated degradation testing.

Table 4-1 Description of the display pattern in each TV set

Panel	Temperature Condition	Initial luminance intensity (The number of pattern)				Total number of patterns
		×1	×2	×4	×6	(128)
#1	25℃	7	7	6	8	28
#2	25℃	7	7	7	7	28
#3	25℃	7	7	7	7	28
#4	40℃	7	7	7	7	28
#5	40℃	7	7	7	7	28
#6	40℃	7	7	7	7	28

was internally maintained during the testing. White OLED panels have a WRGB sub-pixel structure. In order to emit a gray color, the initial luminance intensity of three components (i.e., red, green, and blue) in a single pixel must be identical [97]. The luminance and the color coordinates in the chromaticity diagram (x, y) were measured in each pattern at variable intervals between 24 hours and 180 hours. A Yokogawa multimedia display tester (Model 3298F) was used for luminance measurement. Measurements were conducted until the operating time reached 1,500 hours. Simultaneously, the surface temperature of each OLED panel was measured at identical intervals.

Figure 4-2 briefly presents the direction of color shift in some patterns. As mentioned in section 3.3.2, a unique tandem structure of OLED panels white color coordinate of OLED panels shifts to warm white because the luminance of blue is

lower than that of R/G emission on aging. The bold line in right side of Figure 4-2 is the Prankian locus; the dashed line is the 13th 1, 3, and 7-step MacAdam ellipse, as explained in Figure 3-3 and Table 3-1. The color shift of four patterns (7th , 8th , 9th , and 12th pattern of each OLED panels) were displayed in Figure 4-2.

As shown in Figure 4-3, the difference between the maximum and minimum surface temperatures in same oven temperature condition was 10°C or higher. In some cases, the difference was as high as 15°C.

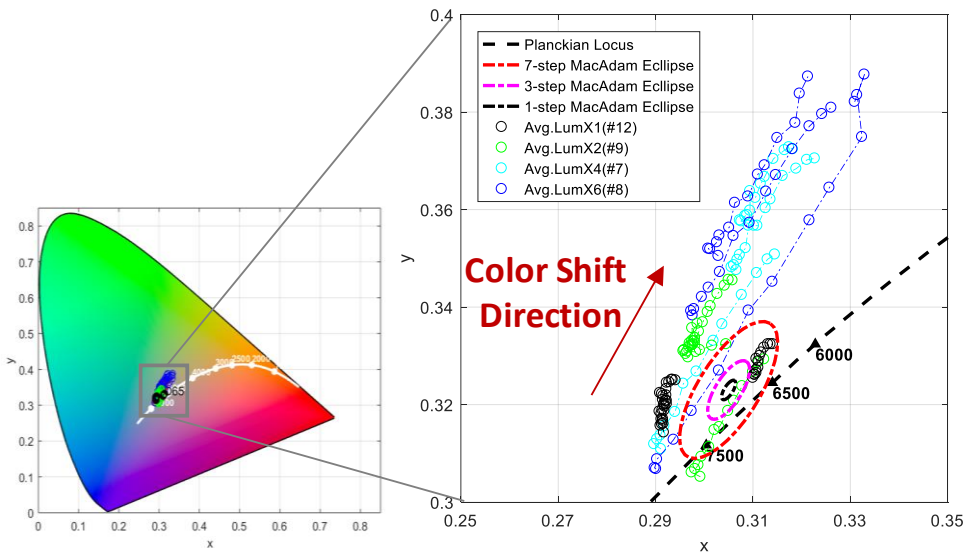

Figure 4-2 Test results of color shift in four patterns of OLED panels.

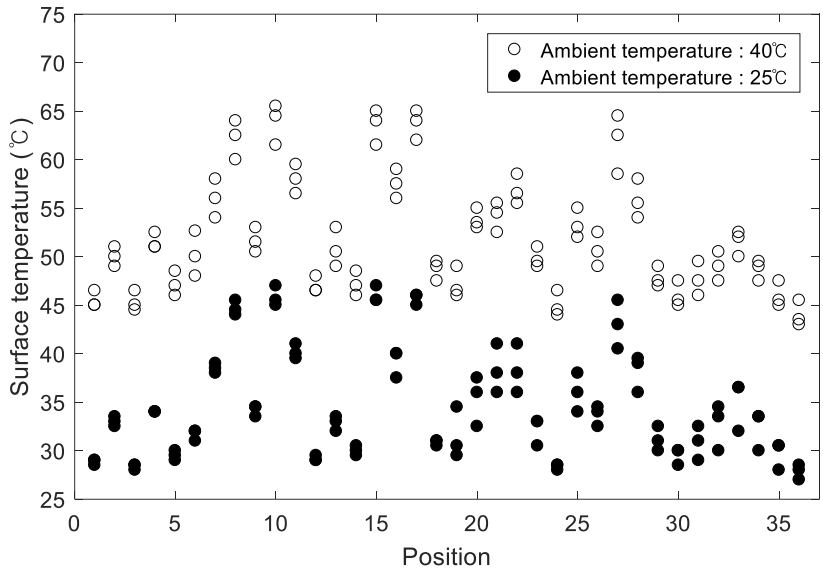

(a) Temperature deviation according to pattern identification

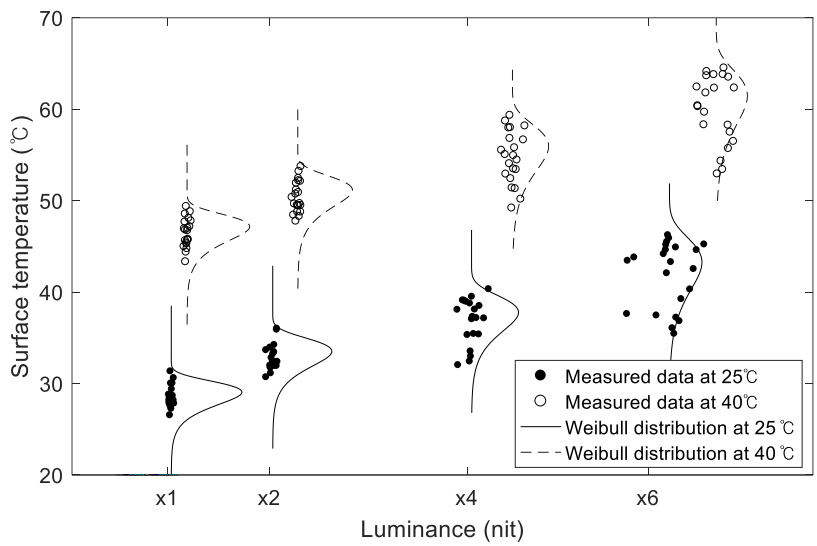

(b) Temperature deviation according to luminance intensity

Figure 4-3 Temperature deviation in the OLED panel at each ambient temperature; Position 1 corresponds to the spot in the top-left corner of the panel, while Position 36 is the spot in the bottom-right of the panel.

4.2 Definition of the Time to Failure

4.2.1 The Time to Failure of Luminance

In this study, 50% or less than the initial luminance intensity was defined as failure of the OLEDs [7, 115, 116]. This type of failure is regarded as “soft failure” because the units are still working; however, they are unacceptable for users. Figure 4-4 – which uses a normalized luminance for the ordinate – shows the test results with curve fitting obtained using the SED model in Equation (3.2). The solid line is

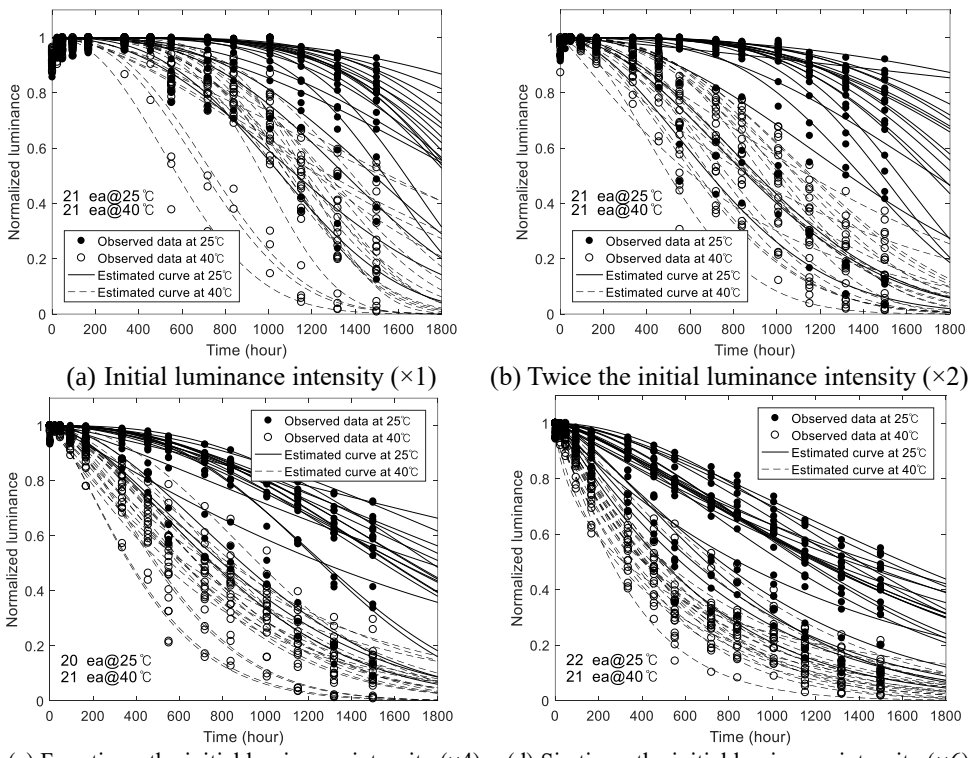

(a) Initial luminance intensity (×1) (b) Twice the initial luminance intensity (×2)

(c) Four times the initial luminance intensity (×4) (d) Six times the initial luminance intensity (×6)

Figure 4-4 Luminance degradation test and curve fitting results.

the SED curve that is estimated from the data at room temperature, while the dashed line is that estimated using the data at 40°C. We found that R-square values were between 0.962 and 0.991. This indicates good agreement between the experimental data and the curve-fitting results. Using the individual SED curve, the time to failure (TTF, t_f; time to 50% performance degradation) was calculated.

4.2.2 The Time to Failure of Color Shift

As described in Chapter 3.1, the time-to-failure of color shift (TTF, t_{f_c}) is defined as the time when the accumulated color shift (Δxy) reaches 0.0322. It is hard to exactly define accumulated color shift due to (1) unstable color perturbation at low luminance intensity and (2) measurement error. In this study, we suggest the projection of a color shift rate vector ($\overrightarrow{xy_i}$) onto a regression vector (**R**) in *xy* chromaticity coordinates. Accordingly, the accumulated color shift is expressed:

$$\Delta xy = \sum_{i=1}^{n-1} \frac{\mathbf{R} \cdot \overrightarrow{xy_i}}{\|\mathbf{R}\|} \tag{4.1}$$

where *n* is the number of measurements. The measured color shift results in the 7th pattern of Set ID 1 at a 40°C temperature condition, as shown in Figure 4-5. The red arrow represents the accumulated color shift at the first duration (Δxy_1), and shows the projection of the color shift rate vector ($\overrightarrow{xy_1}$) onto the regression vector (**R**).

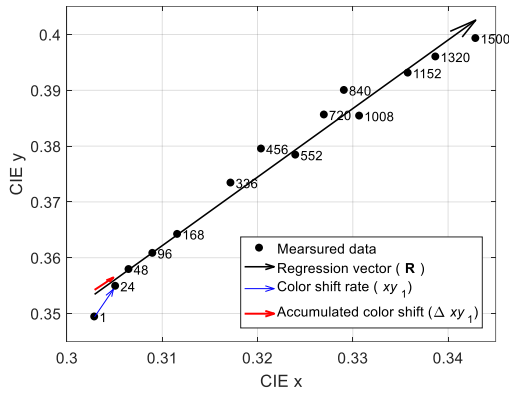

Figure 4-5 Test results of color shift in the 7th pattern of Set ID #1 at a 40℃ temperature condition over time.

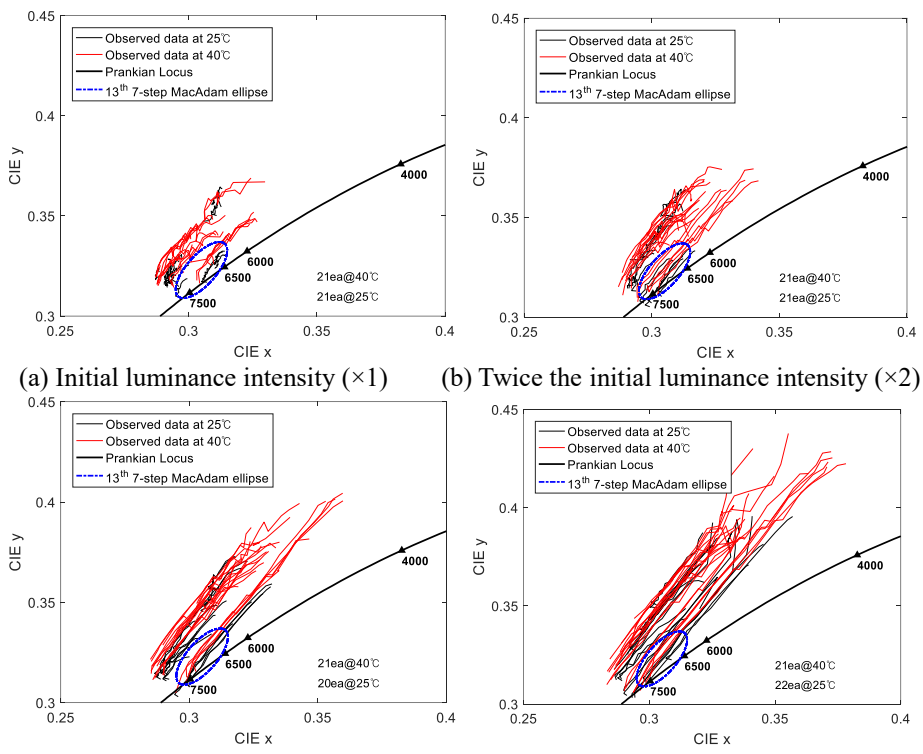

(a) Initial luminance intensity (×1) (b) Twice the initial luminance intensity (×2)

(c) Four times the initial luminance intensity (×4) (d) Six times the initial luminance intensity (×6)

Figure 4-6 Test results of color coordinates in each accelerated condition.

Figure 4-6 shows the test results expressed in the CIE 1931 (x, y) coordinates. It is shown that the higher the initial luminance intensity and ambient temperature, the further the color coordinates were shifted from the initial point over the 1,500 hours. The gray color tended to shift in the yellow direction at each condition, due to the shorter lifetime of the blue EL unit than that of the R/G EL units. The bold line in Figure 4-6 is the Prankian locus, the triangle marks (▲) are each correlated color temperature (CCT), and the dashed blue line is the 13th 7-step MacAdam ellipse, as explained in Figure 3-3 and Table 3-1.

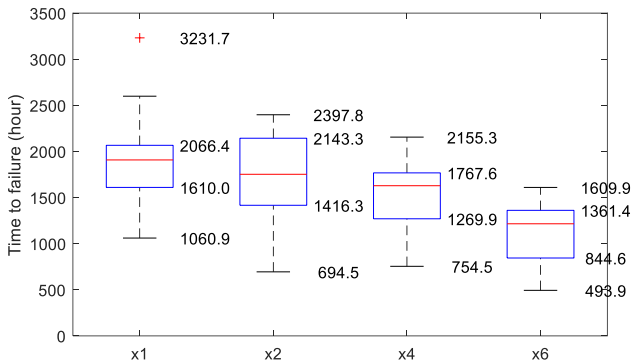

(a) TTF data at 25°C condition

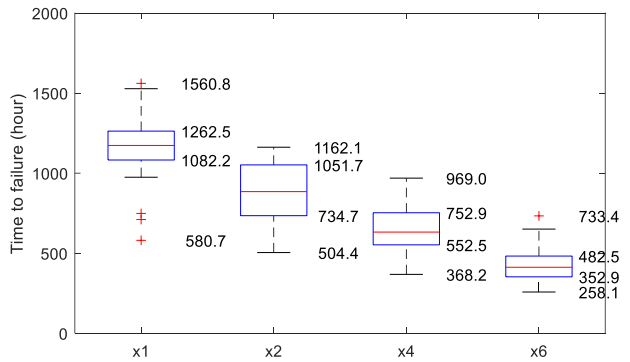

(b) TTF data at 40°C condition

Figure 4-7 Box plot of the time to failure (t_f) estimated from the SED curve.

4.3 Lifespan Test Results

TTF of Luminance (t_f)

A total of 168 TTFs (t_f) – time to 50% performance degradation – were calculated using the estimated SED curve. The mean, along with the 1st, 25th (Q1), 75th (Q3), and 99th percentile TTFs, time to 50% luminance performance degradation are presented in the box plot shown in Figure 4-7. A visual inspection of the results shown in Figure 4-7 allowed qualitative confirmation of the validity of our assumption that the luminance intensity has a inverse relationship with the luminance lifetime. The bottom and top of the box are the first and third quartiles (Q1, Q3); the whiskers represent 1.5 times the interquartile range (1.5×IQR).

TTF of Color Shift (t_{fc})

Figure 4-8, which displays the accumulated color shift for the ordinate, shows the test results with curve fitting obtained by the Power model in Equation (3.3). The results in the figure show that the accumulated color shift rapidly increases in a shorter time as the initial luminance intensity and room temperature are higher. We found that R-square values were between 0.796 and 0.998. This indicates good agreement between the experimental data and the curve fitting results. Using the individual power curve, the failure time, t_{fc} (i.e., time to color shift by 0.0322), was calculated. The mean, along with the 1st , 25th (Q1), 75th (Q3), and 99th percentile

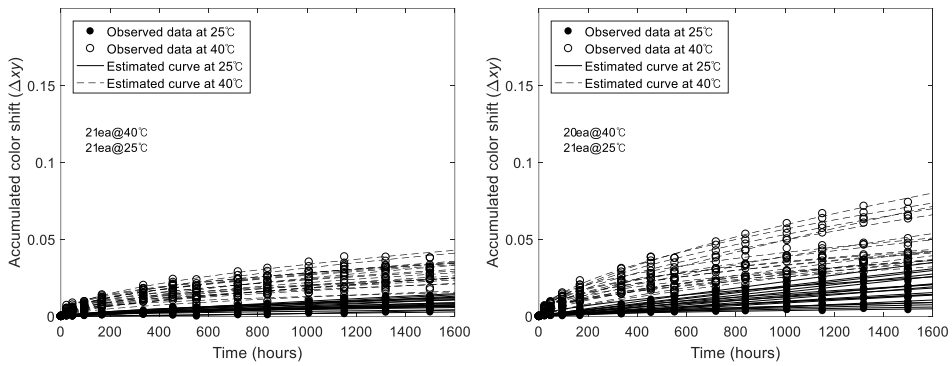

(a) Initial luminance intensity (×1)

(b) Twice the initial luminance intensity (×2)

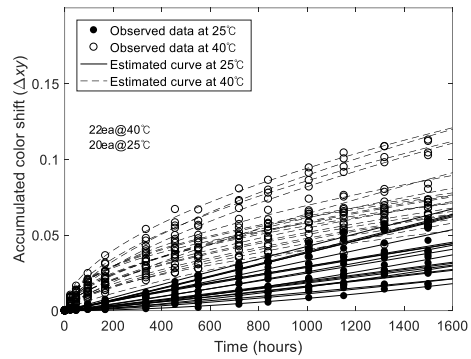

(c) Four times the initial luminance intensity (×4)

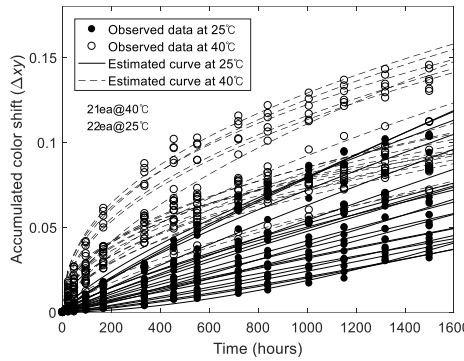

(d) Six times the initial luminance intensity (×6)

Figure 4-8 Test and curve fitting result of color shift estimated from the Power curve.

failure times are presented in the box plot shown in Figure 4-9. The results show that the time to failure dramatically decreases as initial luminance intensity increases. Also, by visual inspection of the box width we can confirm that variation of the time to failure decreases as the acceleration factor increases. The bottom and top of the box are the first and third quartiles (Q1, Q3); the whiskers represent 1.5 times the interquartile range (1.5×IQR) and the '+' symbol indicates outlier data. In this study,

we analyzed the entire data set without discarding outlier data because the outlier data did not have a dominant influence on the distribution type.

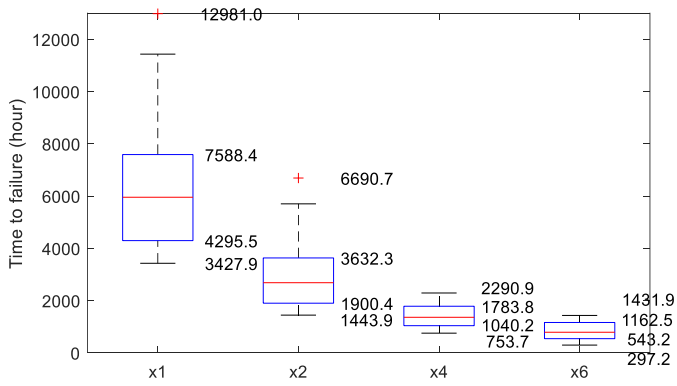

(a)

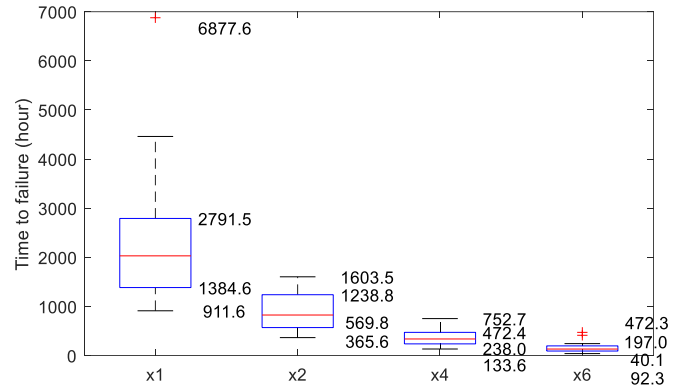

(b)

Figure 4-9 Box plot of the time to failure (t_{fc}) estimated from the Power curve.

Chapter 5. Bivariate Lifetime Model for OLEDs

This chapter presents a novel bivariate lifetime model for OLEDs. TTF data at seven types of accelerated conditions, except data from real-world usage conditions, were utilized to build each bivariate lifetime model for luminance degradation and color shift. Later, data from real-world usage conditions was used for validation of the two bivariate lifetime models.

5.1 Fitting TTF Data to the Statistical Distribution

5.1.1 Estimation of Lifetime Distribution Parameters

In order to determine the proper distribution type, three candidates were considered: normal, log-normal, and Weibull distributions. It was found that the Weibull distribution was most appropriate to represent the TTF data for OLEDs, based on chi-square (χ^2) and Kolmogorov-Smirnov (K-S) goodness-of-fit (GoF) tests. Detailed GoF test results are shown in Table 5-1 and Table 5-2. The observed TTF data and the Weibull distribution of luminance degradation and color shift are shown in Figure 5-1 and Figure 5-2.

The functional form of the Weibull distribution is expressed as:

$$f(t|\beta,\eta) = (\beta/\eta)(t/\eta)^{\beta-1}e^{-\left(t/\eta\right)^{\beta}} \tag{5.1}$$

where β is the shape parameter that directly affects the shape of the failure density distribution curve of the Weibull distribution and η is the scale parameter. The parameters were estimated using the maximum likelihood estimator.

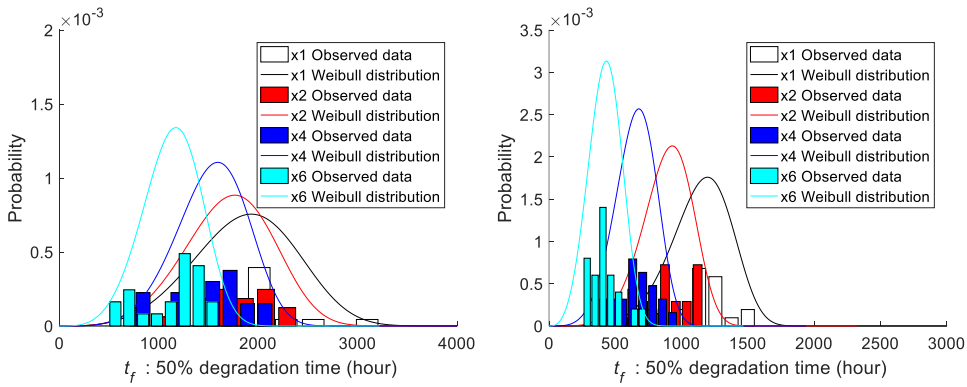

(a) At room temperature (25℃) condition (b) At 40℃ temperature condition

Figure 5-1 The observed lifetime data and the Weibull distribution of luminance degradation.

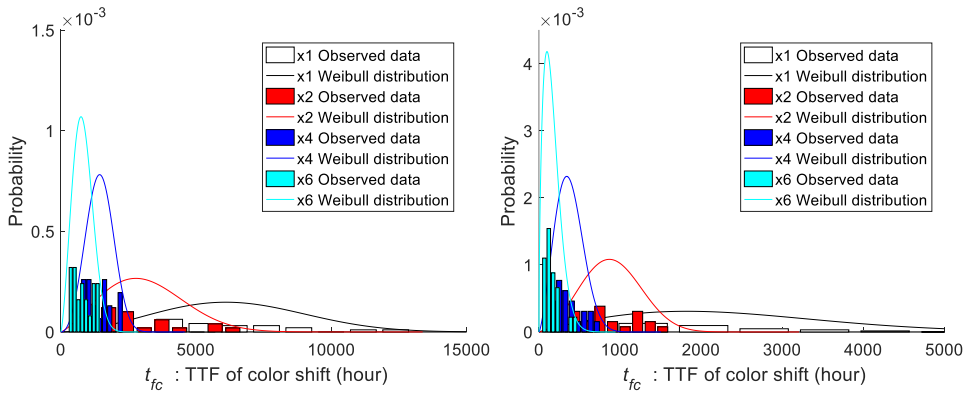

(a) At room temperature (25℃) condition (b) At 40℃ temperature condition

Figure 5-2 The observed lifetime data and the Weibull distribution of color shift.

Table 5-1 Goodness-of-fit test results of luminance TTFs

Temperature	Initial luminance intensity	Type	p-value	
			Chi-square GoF test	Kolmogorov-Smirnov GoF test
25℃		Normal	0.204	0.746
	×2	Lognormal	0.250	0.360
		Weibull	**0.267**	**0.823**
		Normal	0.390	0.354
	×4	Lognormal	0.136	0.145
		Weibull	**0.500**	**0.506**
		Normal	0.204	0.281
	×6	Lognormal	0.147	0.088
		Weibull	**0.273**	**0.397**
40℃		Normal	0.535	0.508
	×1	Lognormal	0.073	0.207
		Weibull	**0.710**	**0.701**
		Normal	**0.999**	0.806
	×2	Lognormal	0.343	0.459
		Weibull	0.785	**0.962**
		Normal	0.839	**0.999**
	×4	Lognormal	0.338	0.890
		Weibull	**0.989**	0.989
		Normal	0.224	0.565
	×6	**Lognormal**	**0.261**	**0.750**
		Weibull	0.189	0.512

* Bold text indicates the maximum value among the three distributions.

Table 5-2 Goodness-of-fit test results of color shift TTFs

Temperature	Initial luminance intensity	Type	p-value	
			Chi-square GoF test	Kolmogorov-Smirnov GoF test
25℃		Normal	0.333	0.458
	×2	**Lognormal**	**0.829**	**0.938**
		Weibull	0.467	0.665
		Normal	0.608	0.829
	×4	**Lognormal**	**0.922**	0.793
		Weibull	0.627	**0.879**
		Normal	0.698	0.822
	×6	**Lognormal**	**0.851**	0.941
		Weibull	0.636	**0.941**
40℃		Normal	0.338	0.397
	×1	**Lognormal**	**0.873**	**0.887**
		Weibull	0.585	0.657
		Normal	0.511	0.665
	×2	**Lognormal**	**0.906**	0.667
		Weibull	0.590	**0.688**
		Normal	0.568	0.597
	×4	**Lognormal**	0.578	**0.976**
		Weibull	**0.714**	0.790
		Normal	0.403	0.571
	×6	Lognormal	0.651	0.941
		Weibull	**0.992**	**0.942**

* Bold text indicates the maximum value among the three distributions.

As shown in Figure 5-3, the shape parameter corresponds to the slope of the Weibull probability paper with $\{\ln t \ \ \& \ \ \ln[-\ln(1-p)]\}$. The scale parameter is the characteristic lifespan that represents the time for 63.2% failure to occur. In Figure 5-3, 21 data representing the usage condition are excluded from those used to build the accelerated model; the estimated usage lifetime is verified in a later step using these data.

The likelihood function is the joint density function of n random variables, given unknown parameters (β, η):

$$L = \prod_{i=1}^{n} f(t_i|\beta,\eta) \tag{5.2}$$

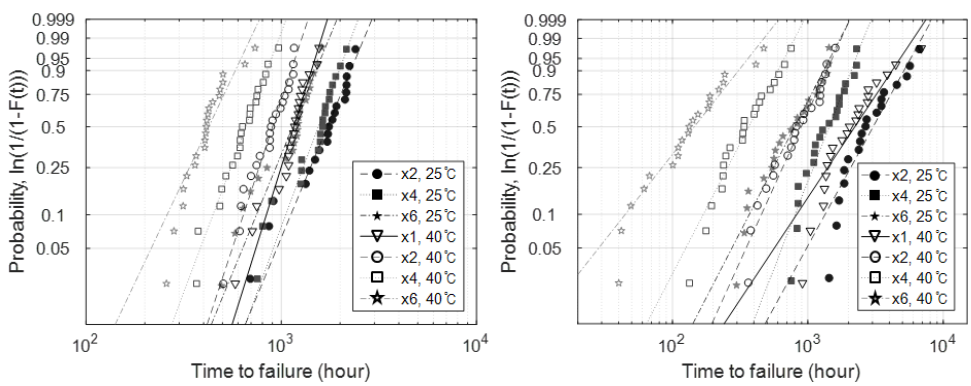

(a) Lifetime distribution of luminance (b) Lifetime distribution of color shift

Figure 5-3 Lifetime distribution plot drawn on Weibull probability paper.

Considering the Weibull parameters, namely the shape and scale parameters, the likelihood function is:

$$L(t_1, t_2, \cdots, t_n|\eta, \beta) = \prod_{i=1}^{n} \frac{\beta}{\eta}\left(\frac{t_i}{\eta}\right)^{\beta-1} e^{-\left(t_i/\eta\right)^{\beta}} \quad (5.3)$$

5.1.2 Estimation of the Common Shape Parameter

The slopes (i.e., shape parameter) in Figure 5-3 show variation. If OLEDs degrade with an identical failure mechanism, the shape parameters should theoretically be identical regardless of the loading conditions. In this study, we assumed that the failure mechanism did not shift, and thus a common shape parameter in the Weibull distribution can be calculated using the maximum likelihood estimator. The logarithm of Equation (5.3) was taken.

$$\ln L(\eta, \beta) = \sum_{j=1}^{n} \ln\left[\frac{\beta}{\eta}\left(\frac{t_j}{\eta}\right)^{\beta-1} e^{-\left(t_j/\eta\right)^{\beta}}\right]$$

$$= n\ln\beta - n\beta\ln\eta + (\beta - 1)\sum_{j=1}^{n}\ln t_j - \sum_{j=1}^{n}\left(\frac{t_j}{\eta}\right)^{\beta} \quad (5.4)$$

where t_j is the failure time in the j^{th} stress level and n is the number of samples.

Then, it was differentiated with respect to η and β.

$$\frac{\partial \ln L}{\partial \eta} = -\frac{n_j \beta}{\eta} + \beta \sum_{j=1}^{n_j} t_{ji}^{\beta} \eta^{-m-1} \tag{5.5}$$

$$\frac{\partial \ln L}{\partial \beta} = \frac{1}{\beta} + \sum_{j=1}^{J} \frac{1}{n_j} \sum_{i \in D_j} \ln t_{ji} - \frac{\sum_{j=1}^{J} \sum_{i=1}^{n_j} t_{ji}^{\tilde{\beta}} \ln t_{ji}}{\sum_{j=1}^{J} \sum_{i=1}^{n_j} t_{ji}^{\beta}} \tag{5.6}$$

where n_j is the number of samples in each stress level (j = 1, 2, …, J); and t_{ji} is the failure time in the i^{th} sample of the j^{th} stress level.

Equations (5.5) and (5.4) are equated to zero. See Equation (5.7) and (5.8):

$$\frac{\sum_{j=1}^{J} \sum_{i=1}^{n_j} t_{ji}^{\tilde{\beta}} \ln t_{ji}}{\sum_{j=1}^{J} \sum_{i=1}^{n_j} t_{ji}^{\beta}} - \sum_{j=1}^{J} \frac{1}{\tilde{\beta}} - \sum_{j=1}^{J} \frac{1}{n_j} \sum_{i \in D_j} \ln t_{ji} = 0 \tag{5.7}$$

$$\tilde{\eta_J} = \left(\frac{1}{n_j} \sum_{j=1}^{n_j} t_{ji}^{\tilde{\beta}} \right)^{1/\tilde{\beta}} \tag{5.8}$$

By solving Equation (5.7) using numerical analysis (e.g., the Newton-Raphson method) a common shape parameter ($\tilde{\beta}$) can be calculated. In this study, the number of stress levels is seven (J=7). For a more graphical understanding of the numerical analysis, Figure 5-4 shows the sum of Equation (5.7) in each stress level according to the common shape parameter. As shown in Table 5-3 and Table 5-4, the common shape parameter was estimated to be 4.67 in the case of luminance degradation and

2.22 in the case of color shift. The corresponding scale parameter was calculated using Equation (5.8). The visual inspection of the slopes shown in Figure 5-5 allowed

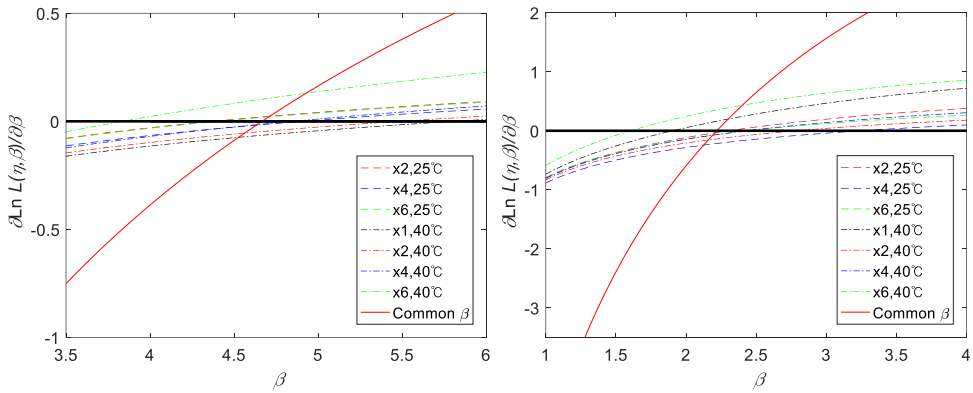

(a) Log-likelihood function of luminance (b) Log-likelihood function of color shift

Figure 5-4 The value of the log-likelihood function according to the common shape parameter ($\tilde{\beta}$).

Table 5-3 Parameter estimation result with maximum likelihood estimation (t_f)

Temperature	Initial luminance	Different shape parameter			Common shape parameter		
		Scale (η)	Shape ($\tilde{\beta}$)	Negative-log likelihood	Scale (η)	Shape ($\tilde{\beta}$)	Negative-log likelihood
25℃	×2	1871.86	4.37	143.50	1881.98		143.56
	×4	1669.20	4.91	139.24	1662.87		139.28
	×6	1243.52	4.41	156.99	1249.39		157.04
40℃	×1	1234.63	5.81	143.87	1216.90	4.6664	144.59
	×2	964.21	5.48	139.77	953.06		140.16
	×4	710.43	4.85	135.09	708.03		135.12
	×6	467.63	3.84	129.43	481.31		130.35

qualitative confirmation of the validity of our assumption, by which a common shape parameter is applied.

Table 5-4 Parameter estimation result with maximum likelihood estimation (t_{fc})

Temperature	Initial luminance	Different shape parameter			Common shape parameter		
		Scale (η)	Shape ($\tilde{\beta}$)	Negative-log likelihood	Scale (η)	Shape ($\tilde{\beta}$)	Negative-log likelihood
25℃	×2	3558.78	2.30	164.068	3531.44		164.092
	×4	1609.80	3.24	151.859	1535.98		153.846
	×6	927.30	2.44	160.120	912.08		160.276
40℃	×1	2696.06	1.90	178.217	2818.99	2.2189	178.767
	×2	1018.53	2.78	152.756	985.72		153.522
	×4	425.95	2.43	136.320	418.85		136.334
	×6	182.17	1.60	124.539	202.95		126.981

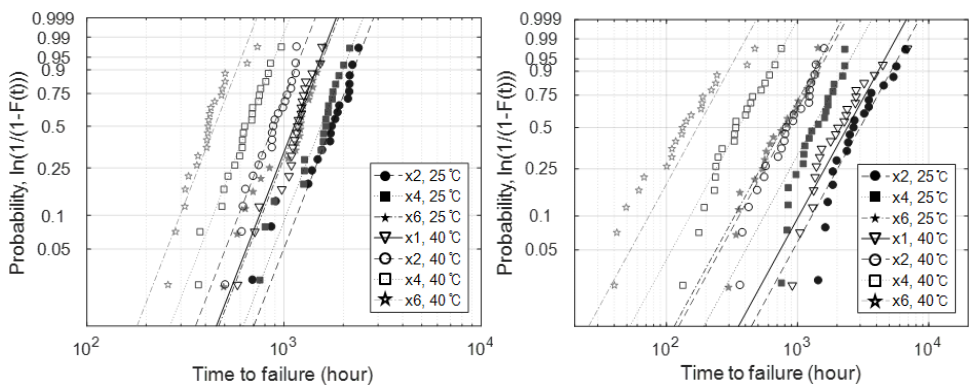

(a) Lifetime distribution of luminance (b) Lifetime distribution of color shift

Figure 5-5 Lifetime distribution plot drawn on Weibull probability paper.

5.1.3 Likelihood-Ratio Analysis

The likelihood ratio test [117] was employed to quantitatively verify the assumption that lifetime distributions under different loading conditions have a common shape parameter for the accelerated degradation testing (ADT) of OLEDs. The null hypothesis is that Weibull distributions at different stress levels have a common shape parameter ($\tilde{\beta}$):

$$H_0: \beta_1 = \beta_2 = \cdots = \beta_J = \tilde{\beta} \tag{5.9}$$

The alternative hypothesis (H_1) is that shape parameters at different stress levels are not the same. The function of test statistics (Λ) is defined as:

$$\begin{aligned} \Lambda &= 2\left(\widehat{\Lambda}_1 + \cdots + \widehat{\Lambda}_J - \widehat{\Lambda}_0\right) \\ &= 2\log L(\hat{\eta}_1, \hat{\eta}_2, \cdots, \hat{\eta}_J, \hat{\beta}_1, \hat{\beta}_2 \cdots, \hat{\beta}_J) - 2\log L\left(\tilde{\eta}_1, \tilde{\eta}_2, \cdots, \tilde{\eta}_J, \tilde{\beta}\right) \end{aligned} \tag{5.10}$$

where $\widehat{\Lambda}_1$, …, and $\widehat{\Lambda}_J$ are the likelihood values obtained by fitting a distribution to the data from each test stress level; and $\widehat{\Lambda}_0$ is obtained by fitting a model with the common shape parameter and a scale parameter for each stress level. The distribution of Λ follows a chi-square distribution with J-1 degrees of freedom (J: DOF of the alternative hypothesis, 1: DOF of the null hypothesis), where J is the number of stress levels. If Λ is equal to or less than $\chi^2(1\text{-}\alpha; J\text{-}1)$, H_0 is accepted, where $\chi^2(1\text{-}\alpha; J\text{-}1)$ is the $100(1\text{-}\alpha)$ percentile of the chi-square distribution with J-1 degrees of

freedom. Otherwise, H_0 is rejected. Using the results in Table 5-3 and Table 5-4, Λ are calculated to be 4.43 in luminance and 12.13 in color shift, which are less than 12.59 (= $\chi^2(0.95; 6)$). Because the calculated value is smaller than the criterion of the chi-squared statistics, it was concluded (with a significance level of 5%) that the shape parameter estimates are not significantly different. Therefore, through visual inspection of Figure 5-5 and the likelihood ratio test, the assumption that the lifetime distributions have a common shape parameter is valid. The results are summarized in Table 5-5 and Table 5-6. Consequently, the mean time to failure (MTTF) at each accelerated condition is obtained as:

$$MTTF = \int t f(t|\tilde{\beta}, \tilde{\eta_J})\, dt = \tilde{\eta_J} \Gamma\left(1 + \frac{1}{\tilde{\beta}}\right) \tag{5.11}$$

Table 5-5 Results of goodness-of-fit test and estimated MTTF of luminance degradation using a common shape parameter

Temperature	Initial luminance	p-value		Estimated Mean time to failure (MTTF)
		Chi-square GoF test	KS GOF test	
25℃	×2	0.34	0.80	1721.07
	×4	0.44	0.42	1520.70
	×6	0.34	0.50	1142.57
40℃	×1	0.42	0.24	1112.85
	×2	0.93	0.69	871.57
	×4	0.92	0.99	647.50
	×6	0.06	0.16	440.16

Table 5-6 Results of goodness-of-fit test and estimated MTTF of color shift using a common shape parameter

Temperature	Initial luminance	p-value		Estimated mean time to failure (MTTF)
		Chi-square GoF test	KS GoF test	
25℃	×2	0.53	0.76	3127.64
	×4	0.73	0.44	1360.35
	×6	0.84	0.98	807.79
40℃	×1	0.28	0.42	2496.65
	×2	0.99	0.77	873.01
	×4	0.89	0.96	370.95
	×6	0.24	0.27	179.74

5.2 Bivariate Lifetime Model

5.2.1 Luminance Lifetime Model

As presented in Section 3.2, the dominant AFs for OLEDs are temperature and luminance. Relevant lifetime models for the accelerated factors are the Arrhenius equation and the inverse power law, respectively. In this section, we propose a novel bivariate lifetime model for OLEDs by integrating the two lifetime models. The proposed model is:

$$MTTF(T\ ,\ I_{\mathrm{lum}}) = \frac{A}{T} \cdot e^{\frac{B}{kT}} \cdot e^{I_{\mathrm{lum}}\left(C+\frac{D}{kT}\right)} \tag{5.12}$$

where k is the Boltzmann constant (8.62×10^{-5}); T is the ambient temperature (K); I_{lum} is the initial luminance intensity; and *A*, *B*, *C*, and *D* are the model parameters.

By definition, the AF is:

$$AF = \frac{MTTF_{\mathrm{n}}}{MTTF_{\mathrm{a}}} \tag{5.13}$$

where $MTTF_{\mathrm{n}}$ is the mean time to failure under a normal usage condition; $MTTF_{\mathrm{a}}$ is the mean time to failure under an accelerated condition. When Equation (5.12) is put into Equation (5.13), the AF for the proposed model becomes:

$$AF = \frac{T_{\mathrm{a}}}{T_{\mathrm{n}}} \cdot \exp\left[\frac{B}{k}\left(\frac{1}{T_{\mathrm{n}}} - \frac{1}{T_{\mathrm{a}}}\right)\right] \cdot \frac{\exp\left[I_{\mathrm{lum_n}}\left(C + \frac{D}{kT_{\mathrm{n}}}\right)\right]}{\exp\left[I_{\mathrm{lum_a}}\left(C + \frac{D}{kT_{\mathrm{a}}}\right)\right]} \tag{5.14}$$

where T_{n} is the temperature under a normal usage condition; T_{a} is the temperature under an accelerated condition; I_{lumd} is the initial luminance intensity; and I_{luma} is the accelerated level of luminance intensity.

5.2.2 Color Shift Lifetime Model

Relevant lifetime models for color shift are the Arrhenius equation and the BET equation, respectively. In this section, we propose a novel bivariate lifetime model for OLEDs' color shift by integrating the two lifetime models. The proposed model is:

$$MTTF(T\ ,\ I_{\mathrm{lum}}) = A\left(\frac{I_{\mathrm{lum}}}{\vartheta - I_{\mathrm{lum}}}\right)^{-B} \exp\frac{C}{kT} \tag{5.15}$$

where k is the Boltzmann constant (8.62×10^{-5}); T is the ambient temperature (K); I_{lum} is the luminance intensity; ϑ is the ideal limit of luminance intensity; and A, B, and C are the model parameters.

When Equation (5.12) is put into Equation (5.15), the AF for the proposed model becomes:

$$AF = \left[\frac{I_{\mathrm{lum_n}}}{I_{\mathrm{lum_a}}} \cdot \left(\frac{\vartheta - I_{\mathrm{lum_a}}}{\vartheta - I_{\mathrm{lum_n}}}\right)\right]^{B} \cdot \exp\left[\frac{E}{k}\left(\frac{1}{T_{\mathrm{n}}} - \frac{1}{T_{\mathrm{a}}}\right)\right] \tag{5.16}$$

where T_{n} is the temperature under a normal usage condition, T_{a} is the temperature under an accelerated loading condition, I_{lumn} is the initial luminance intensity, and I_{luma} is the accelerated level of luminance intensity. The first term of Equation (5.16) represents nonlinearity interaction and singularity when luminance reaches ϑ (=11).

5.3 Validation of the Lifetime Model

Luminance Lifetime Model

Least squares regression analysis was conducted to estimate the unknown model parameters of the proposed bivariate lifetime model. As shown in Figure 5-6, by visual inspection, the proposed model showed a good agreement with the experimental data. The proposed model (i.e., straight line) could explain the data

Table 5-7 Least squares regression analysis

Model parameters				Goodness-of-fit			
A	B	C	D	SSE*	R^2	DOF*	MSE*
41.101	0.25	-1.72	0.04	0.0071	0.9948	3	0.0486

* SSE: sum of square error; DOF: degree of freedom; MSE: mean square error

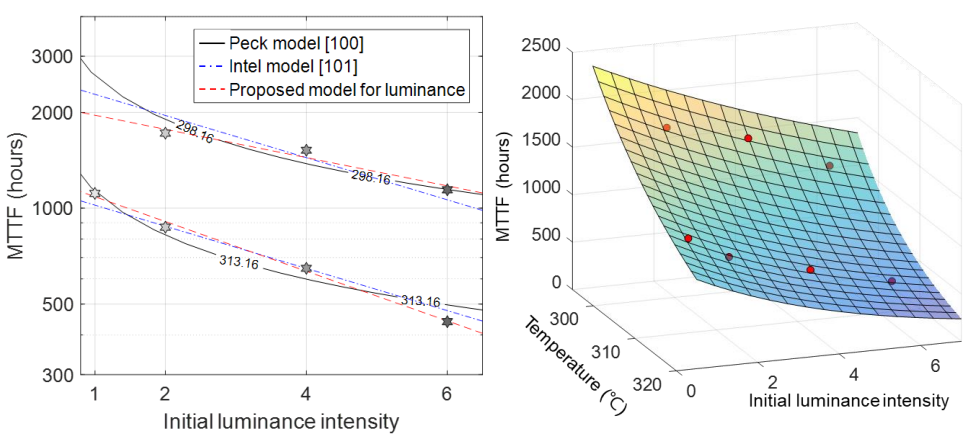

(a) Comparison with each bivariate model (b) Contour plot of the proposed model

Figure 5-6 Regression results of the bivariate luminance lifetime model estimated using MTTF.

sufficiently. Using a quantitative measure, the goodness-of-fit was also evaluated. The R-squared value was as high as 0.9948 (see Table 5-7). From visual inspection and quantitative evaluation, it was concluded that the proposed model was appropriate to describe the relationship between the MTTFs of OLEDs and initial luminance intensity. Figure 5-7 shows how well the two acceleration factors follow the proposed model.

Table 5-8 Acceleration factor at six times the initial luminance intensity

AF	Term 1	Term 2	Term 3*
5.91	1.05	1.59	3.53

* Interaction term with temperature and initial luminance intensity

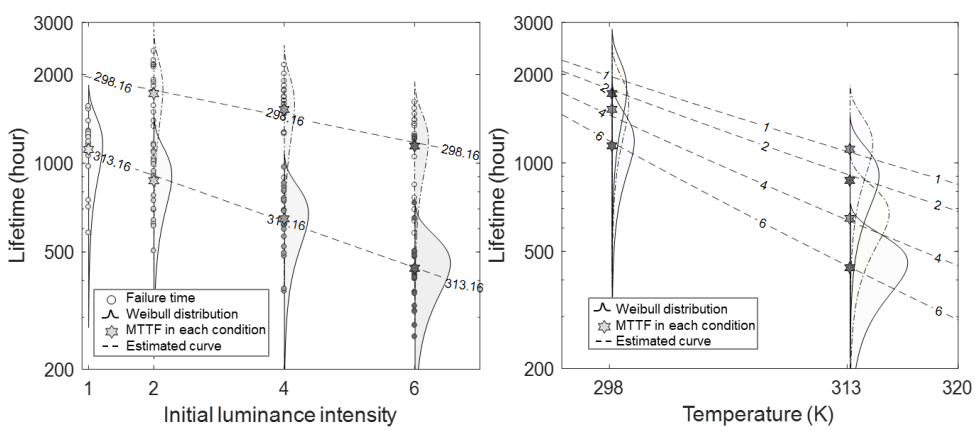

(a) (b)

Figure 5-7 Lifetime distribution calculated from the model and AF: (a) initial luminance intensity and (b) temperature.

The AF between normal usage conditions (i.e., 25°C and initial luminance intensity) and accelerated conditions (i.e., 40°C and six times the initial luminance intensity) was calculated to be 5.91. The details are shown in Table 5-8. The magnitude of the interaction term was largest among all terms, which indicates that a univariate lifetime model with a single AF may provide poor lifetime estimation due to its lack of consideration of the interaction between temperature and luminance.

The accuracy of the proposed bivariate lifetime model was evaluated by comparing the experimental data with statistical distributions calculated by the regression model from seven MTTFs from accelerated conditions. The MTTF was used as a metric for comparison. The MTTF of the 21 failure samples was 1,876 hours; whereas, the MTTF estimated from the proposed model was 1,959 hours. The error was only 4%, which is almost negligible. We also employed two GoF tests to evaluate the validity of the proposed model. Using the estimated MTTF for normal usage conditions and the common shape parameter from Equation (5.11), the scale parameter ($\widetilde{\eta_J}$) was calculated. The statistical distribution at normal usage conditions was estimated using the common shape parameter ($\tilde{\beta}$) and the scale parameter ($\widetilde{\eta_J}$) of the Weibull distribution. The results from chi-square and Kolmogorov-Smirnov GoF tests showed that the statistical distribution predicted from the proposed model was not significantly different from the TTF data with a confidence level of 95%. Therefore, we concluded that the proposed model is valid.

The results from the proposed bivariate lifetime model were compared with those from other models available in the literature. It should be noted that, to the best of our knowledge, no bivariate lifetime model has previously been developed for OLEDs. Therefore, a comparison was conducted with a model used for LEDs and another model used for general applications. First, Han and Wang [6, 12] adopted Peck's relationship [112] to describe the lifetime of LEDs. Second, Intel's model [113] was used in various applications. The model parameters of Peck's and Intel's models were calculated using non-linear regression analysis. The MTTFs estimated using the two models were 2,607 and 2,277 hours, respectively. The errors were 39% and 21%, respectively. The GoF test results showed that the results obtained from the two models were significantly different from the TTF data, which is not acceptable. Consequently, we concluded that the model proposed in this study outperformed the existing models. A summary of the comparison is shown in Table 5-9

Figure 5-8 compares statistical distributions (i.e., probability density and cumulative distribution functions) of OLED lifetime under normal usage conditions. These distributions were obtained from the experimental data and the three models. The results show that the statistical distribution derived from the proposed model best describes the empirical distribution, as compared to other models. This is partially because the proposed model includes the interaction term and is thus more flexible.

Table 5-9 Estimated lifetime and validity check

Model	Estimated lifetime		Chi-square GoF test		KS GoF test	
	$MTTF_{obs}$*= 1875	Error*	Hypothesis	P-value	Hypothesis	P-value
Proposed	1959	4%	Accept	1.66×10^{-1}	Accept	6.38×10^{-2}
Peck's Model	2607	39%	Reject	8.09×10^{-5}	Reject	5.61×10^{-5}
Intel's Model	2277	21%	Reject	8.77×10^{-4}	Reject	4.72×10^{-5}

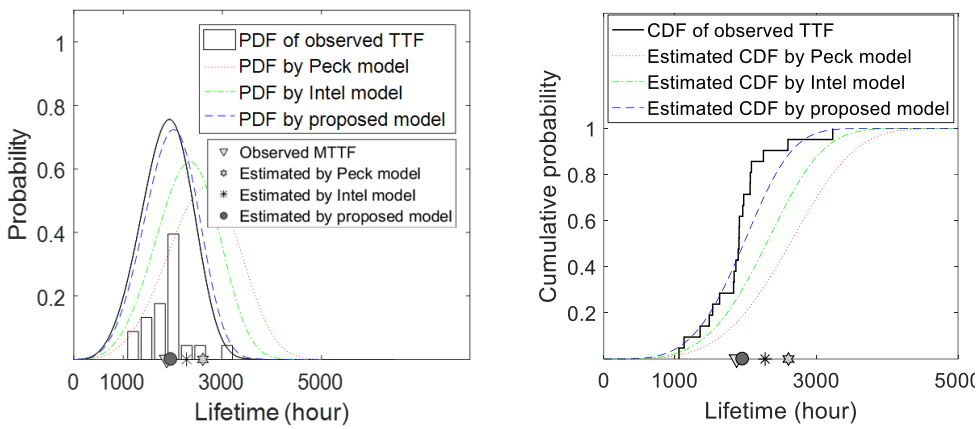

(a) Probability density plot (b) Cumulative distribution plot

Figure 5-8 Comparison between testing and estimated results.

Color Shift Model

Least squares regression analysis, using Equation (5.15), was conducted to estimate the unknown model parameters of the proposed bivariate lifetime model.

As shown in Figure 5-9, by visual inspection, the proposed model showed a good agreement with the experimental data—the proposed model sufficiently explains the data. The R squared value was as high as 0.9770 (see Table 5-10). From visual inspection and quantitative evaluation, it was concluded that the proposed model can appropriately describe the relationship between the MTTFs of OLEDs and initial luminance intensity or ambient temperature. Figure 5-10 shows how well the two acceleration factors follow the proposed model.

Table 5-10 Least squares regression analysis

Model parameters			Goodness-of-fit			
A	B	C	SSE*	R^2	DOF*	MSE*
5.54E-9	-0.8688	0.6622	0.14154	0.9970	4	0.16825

* SSE: sum of square error; DOF: degree of freedom; MSE: mean square error

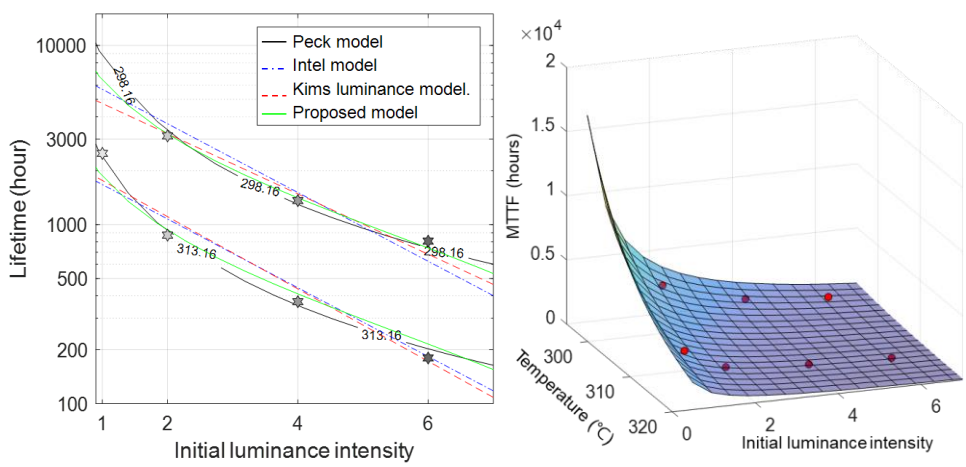

(a) Comparison with each bivariate model (b) Contour plot of the proposed model

Figure 5-9 Regression result of bivariate color shift lifetime model estimated using MTTF.

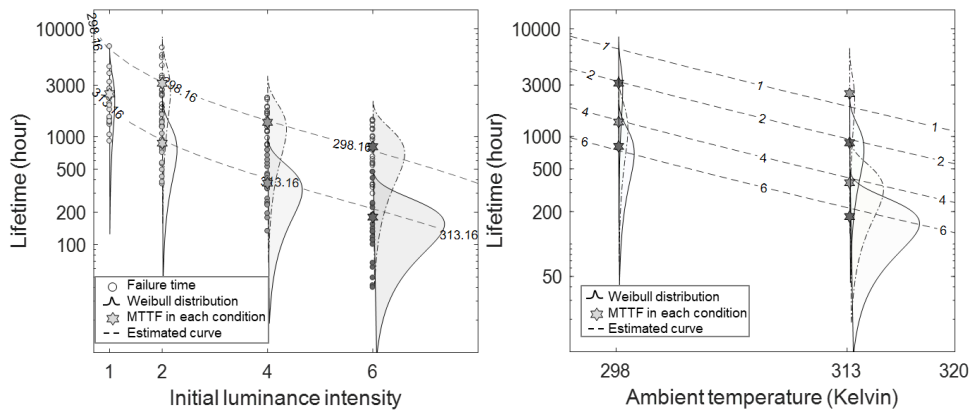

Figure 5-10 Lifetime distribution calculated from the model and AF: (a) initial luminance intensity and (b) temperature.

Table 5-11 Acceleration factor at six times the initial luminance intensity

AF	Term 1	Term 2
29.76	8.66	3.44

The AF between the normal usage (i.e., 25°C and initial luminance intensity) and accelerated (i.e., 40°C and six times the initial luminance intensity) conditions was calculated to be 29.76. The details are shown in Table 5-11. The magnitude of the AF of the color shift was much larger than that of luminance degradation found in the previous section.

The accuracy of the proposed bivariate lifetime model was evaluated by comparing the experimental data with statistical distributions calculated by the

model. The MTTF of the 21 failure samples was 6,450 hours; whereas, the MTTF estimated from the proposed model was 6,400 hours. The error of only 1% was almost negligible. We also employed two GoF tests to evaluate the validity of the proposed model. The statistical distribution for normal usage conditions was calculated using the common shape parameter ($\tilde{\beta}$) of the Weibull distribution. The results from chi-square and Kolmogorov-Smirnov GoF tests showed that the statistical distribution predicted from the proposed model was not significantly different from the TTF data, with a confidence level of 95%. Therefore, we concluded that the proposed model is valid.

The results from the proposed bivariate lifetime model were compared with those from other models available in the literature. It should be noted that, to the best of our knowledge, no bivariate lifetime model for color shift has previously been developed for OLEDs. Therefore, a comparison was conducted with a luminance lifetime model used for LEDs and OLEDs.

The model parameters of Peck's, Intel's, and Kim's models were calculated using non-linear regression analysis. The MTTFs estimated using the three models were 8,692, 5,680, and 4,736 hours, respectively. The errors were 35%, 12% and 27%, respectively. The GoF test results showed that the results obtained from the two models were significantly different from the TTF data, which is not acceptable. Consequently, we concluded that the model proposed in this study outperformed the existing models. A summary of the comparison is shown in Table 5-12.

Figure 5-11 compares statistical distributions (i.e., probability density and cumulative distribution functions) of OLED lifetime for color shift under normal usage conditions. These distributions were obtained from the experimental data and the three models. The results show that the statistical distribution provided by the

Table 5-12 Estimated lifetime and validity check

Model	Estimated lifetime		Chi-square GoF test		KS GoF test	
	$MTTF_{obs}^{*}$= 6450	Error*	Hypothesis	P-value	Hypothesis	P-value
Proposed	6400	1%	Accept	6.66×10^{-1}	Accept	8.64×10^{-1}
Peck's Model	4736	27%	Accept	7.68×10^{-2}	Reject	3.57×10^{-2}
Intel's Model	5680	12%	Accept	5.88×10^{-1}	Accept	5.47×10^{-1}
Kim's Model	8692	35%	Reject	2.60×10^{-3}	Reject	3.60×10^{-3}

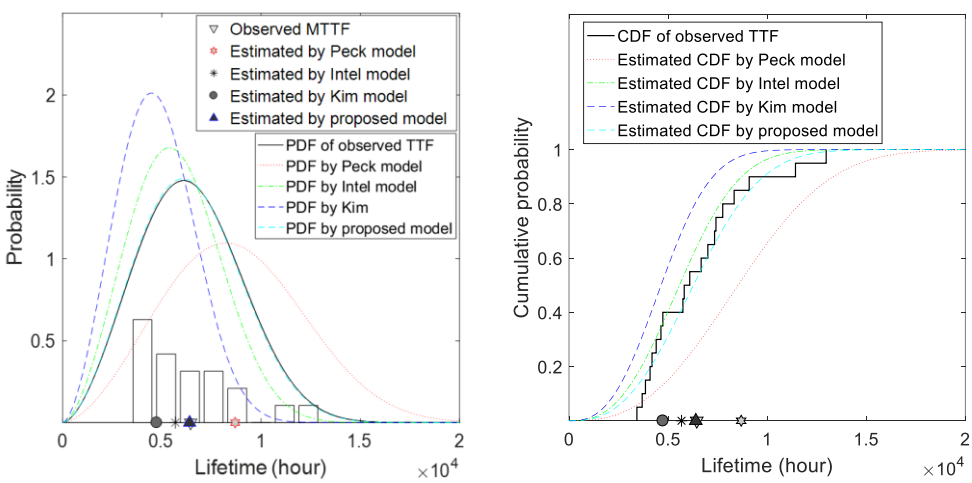

(a) Probability density plot (b) Cumulative distribution plot

Figure 5-11 Comparison between testing and estimated results.

proposed model best described the empirical distribution. This is partially because the proposed model includes the highest nonlinearity interaction term.

Chapter 6. Statistical Model Validation of Heat Dissipation Analysis Model

Ensuring the color shift lifetime for OLEDs is a great hurdle for timely product development. Nonetheless, to date, there has been no effective way to estimate the color shift lifetime at early stages of product development, while the product design is changing. Mechanical engineers and the reliability experts have to execute many tests to gather the best available lifetime estimates.

To address this need, this research proposes a novel scheme for color shift lifetime analysis. The proposed technique consists of: (1) a finite element model for OLED thermal analysis that incorporates the uncertainty of the measured surface temperature, (2) statistical model validation, including model calibration to ensure agreement of the predicted results with respect to experimental data; the model is calibrated through adjustment of a set of physical input variables and a hypothesis-test-based validity check to measure the degree of mismatch between predicted and observed results, and (3) a regression model that can predict the color shift lifetime using the surface temperature at an early stage of product development. It is expected that the regression model proposed here will shorten product development time substantially by predicting the color shift lifetime through OLED thermal analysis.

TV manufacturers face a difficult task when attempting to analyze and design a thermal path or heat dissipation scheme for a TV set. First, they do not have exact information about the amount of thermal dissipation in the OLED microstructure,

nor do they understand the exact effect that temperature conditions have on time-dependent OLED characteristics. Due to the material properties of each stacking layer in the microstructure and the size of the finite element model that would be required, it is virtually impossible to build a detailed thermal analysis model.

Second, test results show significant variability not only among TV samples, but also spatially in individual samples. As shown in Figure 4-3, test results show uneven luminance distribution and spatial temperature variations, even in the same temperature condition. The reason for this randomness is mainly due to the organic materials used and a result of the manufacturing process [118]. Threshold voltage and mobility are uncertain due to the manufacturing process. Localized crystallization on the panel during manufacturing of the low-temperature polycrystalline silicon (LTPS) TFT can easily result in non-uniformity of the OLED current [119-121]. Each pixel has a different threshold mobility value. Also, the reason for TFT degradation is due to characteristic decay of threshold voltage and mobility according to the driving voltage. In order to compensate for threshold voltage and mobility variations, and thereby enhance display uniformity, most commercial manufacturers utilize compensation algorithms and additional compensation circuits [122].

6.1 Estimation Method for TTF using Surface Temperature

Large OLED panels with a size of 55 inches or larger are subjected to physical uncertainty in real-world applications (e.g., spatial temperature variations in the OLED panel and inherent randomness in organic materials). In particular, the orientation, size, and non-uniform temperature profile impacts OLED operation, resulting in an uneven luminance distribution [33, 123, 124].

Some prior research about OLEDs' picture quality has been focused on defining a relationship between temperature and luminance degradation [118, 125]. In this section, we propose an empirical relationship between surface temperature and the TTF from color shift through a regression method, as shown in Figure 6-1. This relationship between surface temperature and the TTF of color shift enables estimation of the TTF of color shift using only temperature data and at the early stages of development.

The proposed model is:

$$t_{f_c} = a_0 e^{a_1 T_j} \tag{6.1}$$

where T_j is temperature on the surface of the OLED panel and a_0 and a_1 are the model parameters. Detailed regression results are shown in Table 6-1. Equation (6.1) can be used to estimate the time to failure of color shift by using the junction temperature.

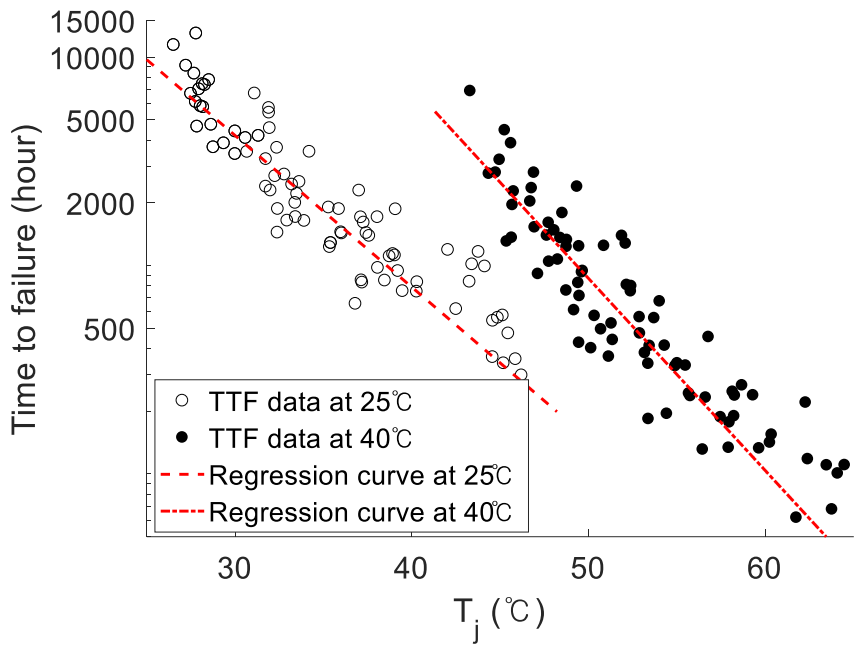

Figure 6-1 Test and regression results: The unfilled circle is the test result at room temperature (25℃); the solid circle is the test result at 40℃. The red line is estimated using the exponential regression model.

Table 6-1 Least squares regression analysis

Temperature	Model parameters		Goodness of test			
	a_0	a_1	SSE*	R^2	DOF*	MSE*
25℃	6.40E+05	-0.1675	4.32E+07	0.9235	79	739.79
40℃	3.51E+07	-0.2121	5.55E+06	0.9469	82	260.25

* SSE: sum of square error; DOF: degree of freedom; MSE: mean square error

6.2 Thermal Analysis Model for OLED Displays

Because thermal design has an effect on various reliability issues in large-sized displays, mechanical designers utilize a computational model in the early stages of

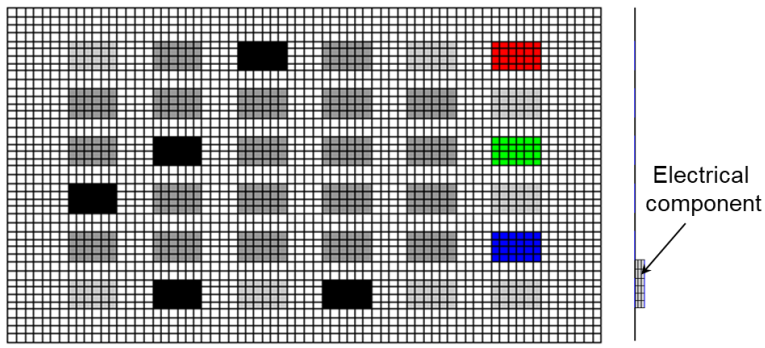

Figure 6-2 Description of finite element model for thermal analysis.

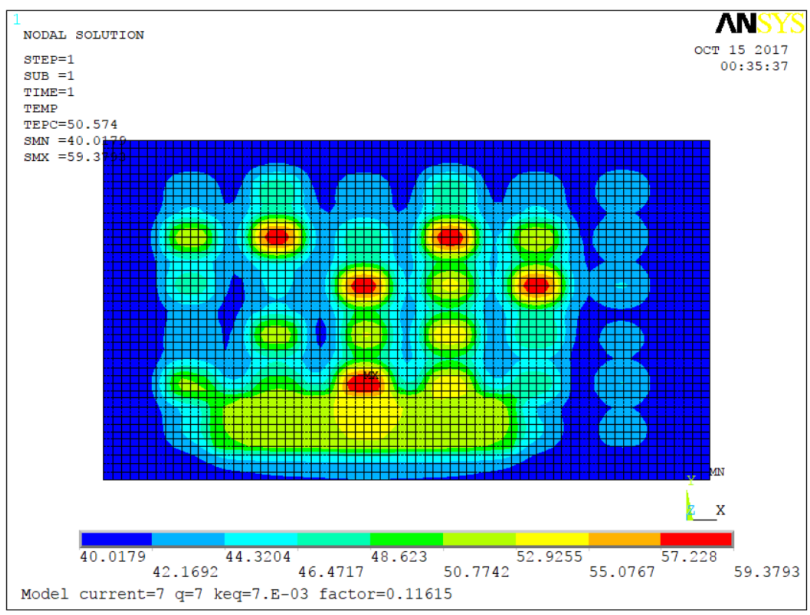

Figure 6-3 Resultant temperature contour of simulation.

product development. Unfortunately, there is a practical obstacle to building a computational model for large-sized OLED TVs due to their complicated micro structure temperature limits. Thus, no model is available to guarantee the various reliability factors related to picture quality.

Computational fluid dynamics analysis of an OLED TV takes 0.5 day with 8 CPU parallel processing to solve the fundamental nonlinear differential equations. Thus, we suggest a simple finite element model for steady-state analysis, as shown in Figure 6-2. The heat transfer coefficient (h) can be scaled as $L_c^{-1/4}$, (the characteristic length of the display in the gravity direction), using a natural convection correlation the Nusselt number has been experimentally fit to the Rayleigh number in the case of the isothermal vertical plate [38]. The convection coefficient was assigned differently according to the vertical location in a commercial FEA package, ANSYS. A simulated temperature result contour is shown in Figure 6-3.

6.3 Statistical Calibration using the EDR Method

The uncertainty of unknown model variable vector ($\boldsymbol{\theta}$) can be represented by statistical parameters of a suitable distribution. The hyper-parameter vector ($\boldsymbol{\Theta}$) is defined as $\boldsymbol{\Theta} = \log N\{\mu_{\boldsymbol{\theta}}, \sigma_{\boldsymbol{\theta}}\}$, which includes the logarithmic mean and standard

deviation of θ. The calibration parameter vector ($\boldsymbol{\Theta}$) will be determined by maximizing the agreement between the predicted and observed results as:

$$\text{maximize} \quad L(\boldsymbol{\Theta}|\mathbf{y}) = \sum_{i=1}^{n} \log_{10}\lfloor f(y_i|\boldsymbol{\Theta})\rfloor \tag{6.2}$$

where y_i is a component of the random response; *n* is the number of observed data; $f(y_i|\boldsymbol{\Theta})$ is the PDF of y_i for a given value of $\boldsymbol{\Theta}$; and *L* is a likelihood function, which is used as the calibration metric to measure the degree of agreement between the predicted and observed data.

After building the PDF of a predicted response using uncertainty propagation (UP) analysis, the likelihood function is calculated by integrating probability densities over experimental data. Among many UP analysis approaches, the eigenvector dimension reduction (EDR) method was utilized in the research outlined in this thesis due to its relatively low computational cost. The EDR method is an enhancement of the univariate dimension reduction method that calculates the statistical moments of the response. The statistical moments of the response, $\hat{Y}$, can be calculated as:

$$\mathbf{E}\left[\hat{Y}^m(\mathbf{Z})\right] = \int_{-\infty}^{\infty}\int_{-\infty}^{\infty} \hat{Y}^m(\mathbf{z}) \cdot f_{\mathbf{z}}(\mathbf{z}) \cdot d\mathbf{z}\,, \qquad m = 0,1,2,\cdots \tag{6.3}$$

where, $\mathbf{Z}$ is an augmented variable vector, $\mathrm{E}[\cdot]$ indicates the expectation operator, and $f_{\mathbf{z}}(\mathbf{z})$ is the joint probability density function (PDF) of $\mathbf{Z}$. Multi-dimensional

integration in Equation (6.3) can be converted into multiple one-dimensional integrations using additive decomposition. The additive decomposition, $\hat{Y}_a$, is defined as:

$$\begin{aligned}\hat{Y}(Z_1,\cdots,Z_N) &\cong \hat{Y}_a(Z_1,\cdots,Z_N)\\ &= \sum_{j=1}^{N}\hat{Y}\left(\mu_1,\cdots,\mu_{j-1},Z_j,\mu_{j+1},\cdots,\mu_N\right)-(N-1)\hat{Y}(\mu_1,\cdots,\mu_N)\end{aligned} \tag{6.4}$$

Although the additive decomposition ($\hat{Y}_a$) ignores all the interactive terms, the produced error is less than that of a second-order Taylor expansion method for probability analysis. Two reasons can explain this observation: (1) the additive decomposition ($\hat{Y}_a$) preserves the accuracy of all uni-variable terms; (2) after the expansion of the true response ($\hat{Y}$) using Taylor expansion at the mean value μ_i, the integration of the interactive variable terms in Equation (6.4) becomes zero, as long as one of the variables is odd-order, provided that all variables are independent and the integration domain is symmetric. The symmetry of the integration domain, namely the symmetric PDF of the variable, ensures that all odd-order central moments are zeros. For that reason, any asymmetric distribution must be transformed to a symmetric distribution. Therefore, the largest error incurred due to the additive decomposition is at the fourth even-order term, producing a negligible error. In aid of the additive decomposition, the probability analysis of the response becomes much simpler. For reliability and quality assessment, the m^{th} statistical moments for the response can be approximately obtained as:

$$\mathbf{E}\left[\hat{Y}_a^m(\mathbf{Z})\right] = \mathbf{E}\left\{\left[\sum_{j=1}^{N} \hat{Y}\left(\mu_1, \cdots, Z_j, \cdots, \mu_N\right) - (N-1)\cdot \mathrm{Z}(\mu_1, \cdots, \mu_N)\right]^m\right\} \qquad (6.5)$$

Using a binomial formula, Equation (6.5) can be evaluated by executing one-dimensional integration recursively. To enhance both accuracy and efficiency in probability analysis, three technical elements are considered: (1) the eigenvector sampling method to handle correlated and asymmetric random input variables, (2) the stepwise moving least squares method for one dimensional response approximation, and (3) a stabilized Pearson system for generating a PDF of a response. Thus, for N number of random variables, the EDR method only demands 2N+1 or 4N+1 eigenvector samples to obtain a PDF of a response.

In this thesis, *n* is 84 (3 sets and twenty-eight patterns per set), because we utilized three OLED panels tested at 25℃ ambient temperature for the statistical calibration procedure. We used a gradient-based optimizer in MATLAB software to solve the calibration problem. Uncertainty propagation (UP) analysis using the approximate integration method was achieved by: (1) calculating the statistical moments of the system response, and (2) constructing the statistical distributions of the system response. We applied the eigenvector dimension reduction (EDR) approximate integration technique, which required only 4N+1 runs for a single iteration [87, 126]. The Pearson system was implemented for construction of the statistical distribution [85, 87, 127]. The statistical calibration procedure is drawn in Figure 6-4.

Statistical calibration begins with the selection of unknown variables. The selection of an appropriate set of unknown variables is critical to the successful implementation of model calibration. We defined three unknown variable candidates (N=3) based on both expert opinions and historic development data. Each of them is assumed to follow a specific statistical distribution with two parameters.

The first unknown variable, the amount of driving current (j_1) that generates light while it dissipates heat, is known to have a liner relationship with luminance intensity. Figure 4-3 shows both the variance of luminance and surface temperature in the same condition, according to pattern location. In this study, we assumed that the driving

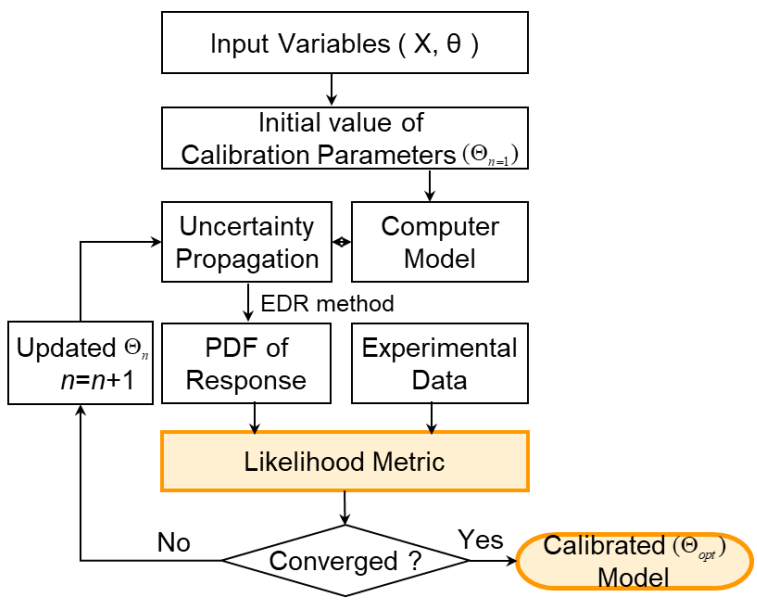

Figure 6-4 The statistical calibration procedure.

current has uncertainty that was modeled by a log-normal distribution with two parameters ($\theta_1 = j_1 \sim \log N(\mu_{\theta_1}, \sigma_{\theta_1})$).

The second unknown variable is the amount of heat dissipation (q_{pcb}) from the printed circuit board (PCB) that is attached to the back side of the OLED panel ($\theta_2 = q_{\mathrm{pcb}} \sim \log N(\mu_{\theta_2}, \sigma_{\theta_2})$).

The last variable is the deviation of the equivalent thermal conductivity (k_{eq}) of the overall OLED panel. Based on thermal designers' experience and the literature, the mean of the equivalent thermal conductivity was set as 4.78 W/℃/m^2 (see reference [33]). Because individual OLED pixels in a panel are subjected to various physical and operating uncertainties, the distribution of conductivity was assumed to be a log-normal distribution ($\theta_3 = k_{eq} \sim \log(4.78, \sigma_{\theta_3})$).

6.4 Validity Check

A validity check of a statistically calibrated model requires experimental data under different operating conditions. The experiments required for a validity check are normally conducted under various operating conditions in a validation domain. Given limited experimental data for the validity check, it is beneficial to integrate evidence from all observation data over the entire validation domain into a single measure of overall mismatch. The U-pooling method allows integration of the

evidence from all experimental data under various experimental settings [85, 128]. The cumulative density, u_i, can be obtained through the transformation of every experimental datum (y_i) described in Section 2.4. The u_i values obtained using (1) all experimental data and (2) the predicted results of the computational model follow a uniform distribution of [0,1]. Figure 6-5 shows an example of the experimental datum (y_i) in the 8th pattern and the cumulative density (u_i) calculated from the predicted PDF. A total of 84 temperature data (3 OLED sets and twenty-eight patterns per set) at an ambient temperature condition, were utilized for the calibration domain.

We can quantify the degree of mismatch between the dispersion of experimental data and the distribution of the predicted result by calculating the area (U_m) between

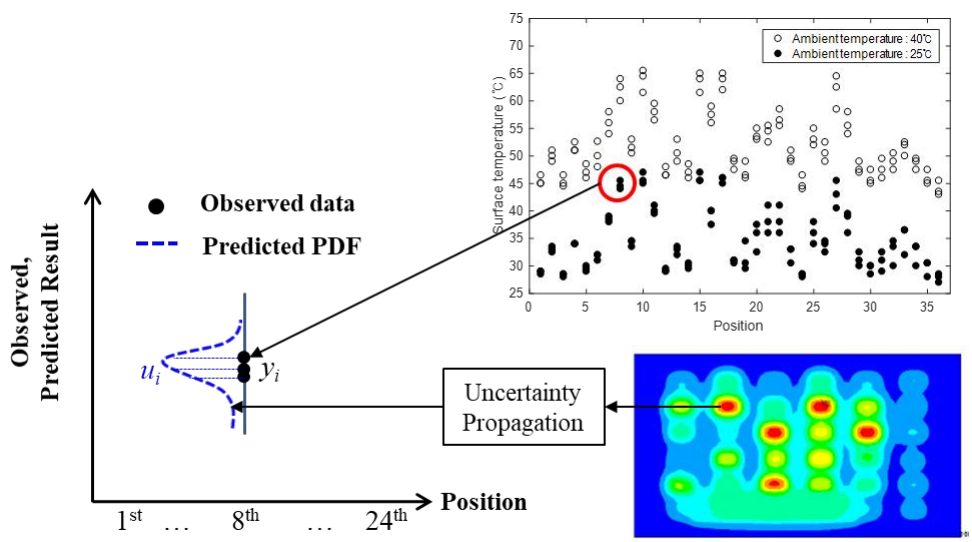

Figure 6-5 The transformation of experimental temperature (y_i) from the predicted PDF estimated by the simulation result.

the CDF of the uniform distribution (F_{uni}) and the empirical CDF (F_u) of the u_i values corresponding (y_i) to the experimental data. In the research outlined in this thesis, there are eighty-four experimental data; the predicted PDFs under different conditions (different positions in the three different OLEDs) are shown in Figure 6-6(a). The u_i of each experimental datum was calculated and its empirical CDF is drawn in Figure 6-6(b). The calculated area of the shaded region in Figure 6-6(b) indicates the U_m. The smaller the calculated the U_m, the closer the predicted PDF is to the actual distribution of experimental data. For example, if the model well represents the physical responses (i.e., the model is valid) the U_m will be zero when enough experimental data exists. Otherwise, (i.e., when the model is not valid), the U_m will be a positive value. An area metric enables us to verify whether the predicted temperature at each pattern of the OLED panel under the 40℃ condition, using the calibrated parameters at the 25℃ condition, is valid.

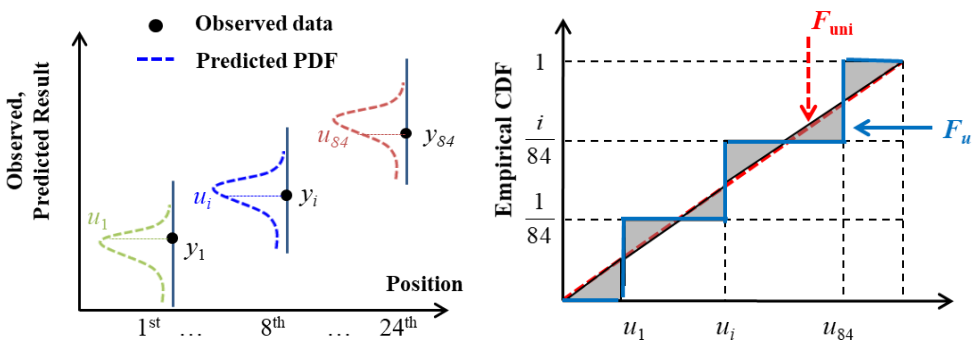

(a) Predicted and experimental results (b) Area metric (=U_m)

Figure 6-6 Calculation of area metric.

6.5 Results and Discussion

Figure 6-7 compares the initial PDFs of surface temperature with the calibrated PDFs that are acquired through uncertainty propagation analysis using the EDR method. The calibrated vector of the unknown variables and the value of likelihood are listed in Table 6-2. Using the calibrated vector under a 25℃ temperature condition, we performed a validity check of 84 observed data in the validation domain under a 40℃ temperature condition. Eighty-four U-pooling and area metrics, both in the calibration and the validation domains, were individually plotted

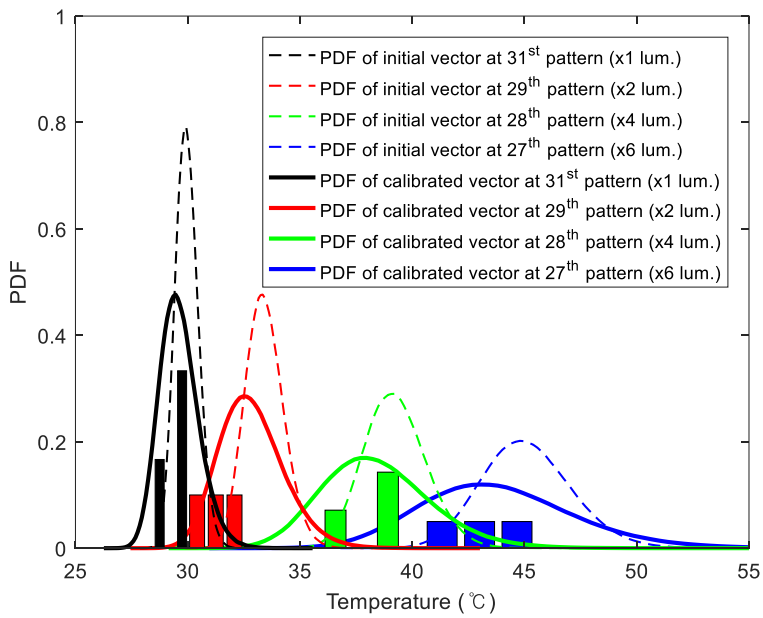

Figure 6-7 Initial guess and calibrated values for surface temperature at the 27th, 28th, 29th, and 31st pattern of three OLED panels under a 25℃ temperature condition.

in Figure 6-8. The values of the area metric in each validation (U_{m_v}) and calibration domain (U_{m_c}) were 0.06096 and 0.03943.

A hypothesis test for the validity check proposed by Jung et al. [85] was implemented using the empirical probability distribution of area metric ($f_{u,i}$).

Table 6-2 The calibrated vector of the unknown variables

Variables	Random Parameter	Initial vector	Calibrated vector
The amount of driving current (j_1)	Mean	9	8.33
	Std.	0.9	1.5
The amount heat dissipation (q_{PCB})	Mean	2.5	2.73
	Std.	0.25	1.5
Equivalent conductivity (k_{eq})	Mean	0.48	1.2
Negative log-likelihood		126.67	70.74

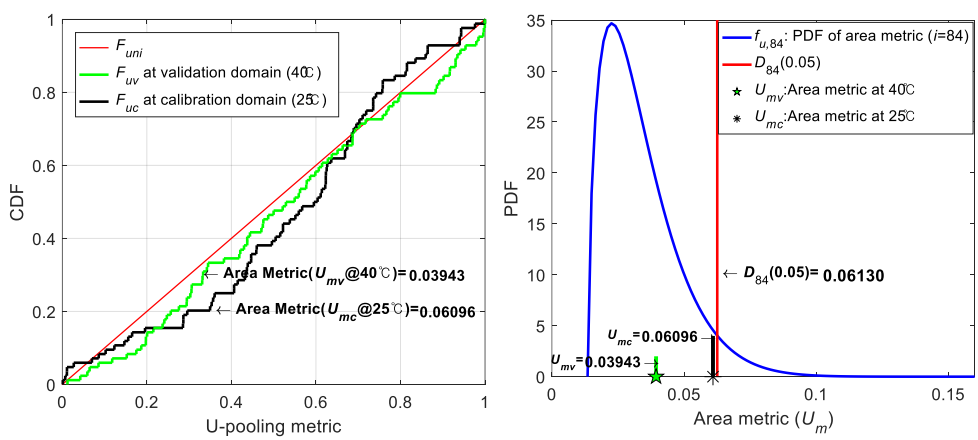

Figure 6-8 Area metric and hypothesis results obtained with 84 test results in the calibration and validation domains.

Results show (1) it asymptotically converges to zero as the size of the experimental data increases, and (2) it is identically determined irrespective of the shape of the true distribution because a set of u_i values always follows a uniform distribution regardless of the true distribution shape. Both area metrics are less than 0.0613 ($D_{84}(0.05) = f_{u,84}$). Since the calculated values are smaller than the criterion of the area metric (U_{m_v} and $U_{m_c} < D_{84}(0.05) = 0.0613$), it was concluded that the calibrated model is valid even in the validation domain.

Chapter 7. Case Study

For the demonstration of reliability estimation at an early stage of product development, this chapter employs a case study about thermal heat dissipation analysis.

7.1 Computational Modeling

Computational fluid dynamics (CFD) uses numerical method to solve the fundamental nonlinear differential equations that describe fluid flow. This enables accurate prediction of temperature as it considers all modes of heat transfer. Figure

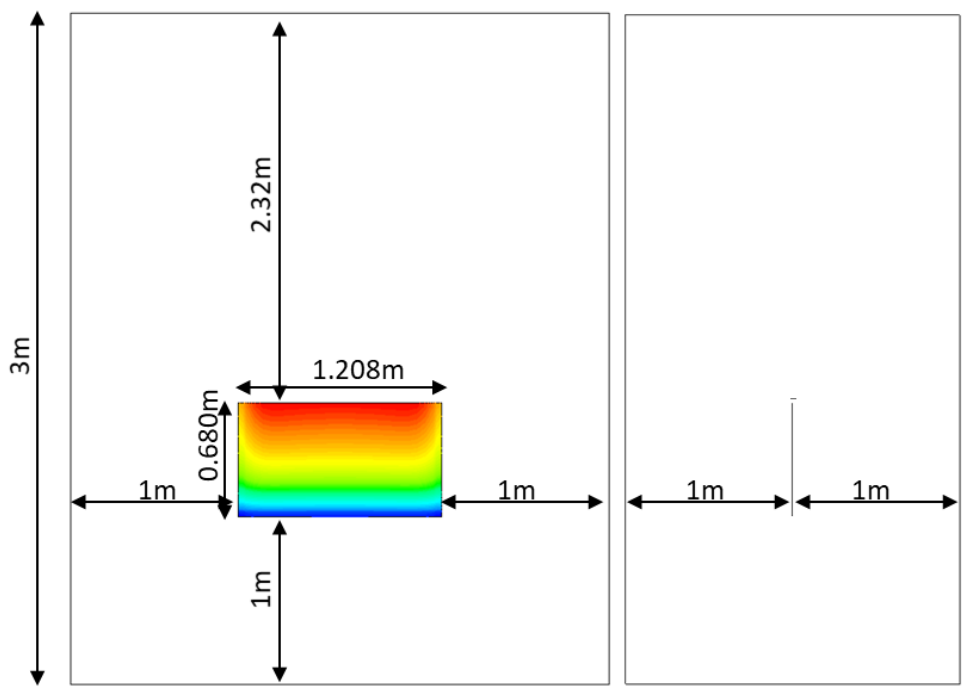

Figure 7-1 Top view of simulation domain (left) and side view (right)

7-1 shows the simulation domain of CFD analysis of OLED panels. A 55-inch OLED panel employing WOLED and oxide TFT was implemented inside of the simulation domain. The size of OLED panel is 1.2m × 0.68m with 10mm thickness, and the simulation domain is 3.2m × 2m × 3m. CFD analysis was performed in the commercial CFD package, ICEPAK. In order to natural convection phenomenon,

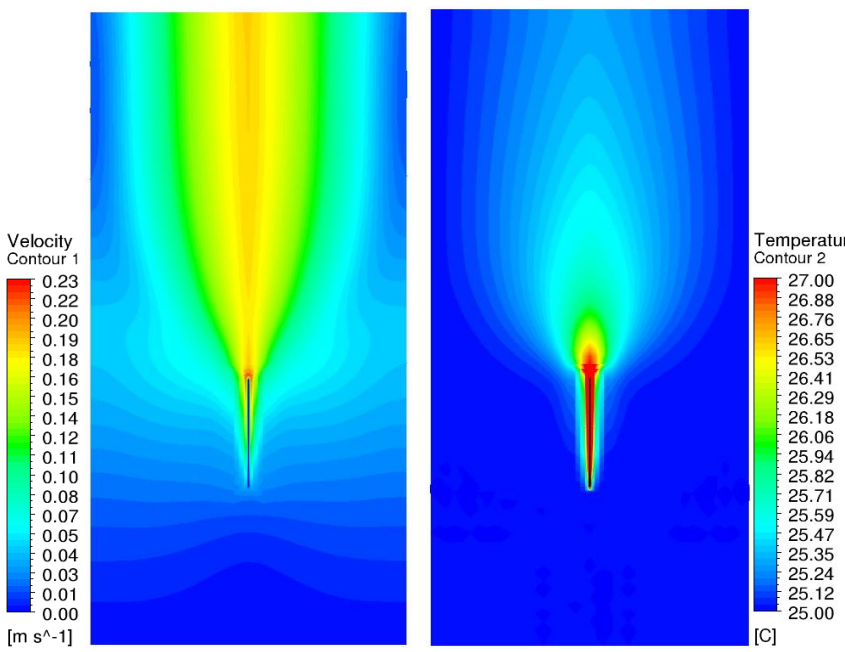

(a) Velocity result of fluid domain (b) Temperature result of fluid domain

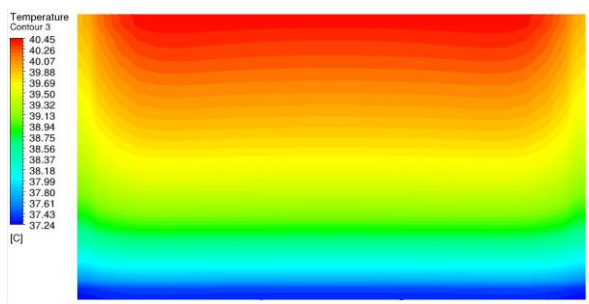

(c) Temperature result in OLED panel

Figure 7-2 Simulation results: (a) Velocity of fluid domain, (b) Temperature of fluic

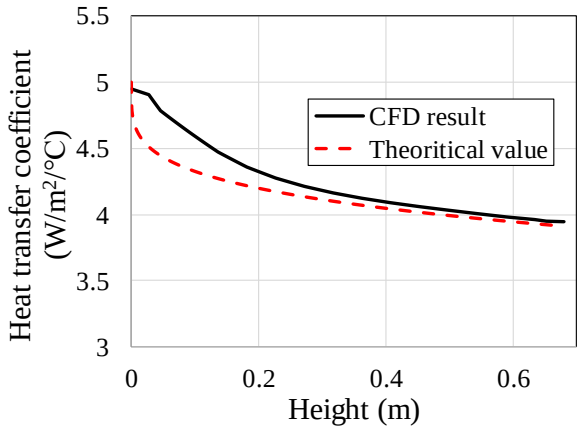

Figure 7-3 The comparison between the heat transfer coefficient from CFD result and from theoretical value.

both of the momentum term and the energy term was solved together. The radiation effect was neglected because temperature change is not high. As shown in Figure 7-2(c), the maximum temperature of panel reaches on the top of the panel.

In order to validate the heat transfer coefficient (h) calculated from theorical value, the heat transfer coefficient in each surface node was extracted from CFD result. Figure 7-3 shows the comparison of the heat transfer coefficient (h) along to virtical direction. The theoritcal value of the heat transfer coefficient fit approximately well, even though there is mismatch in bottom area of OLED panel.

7.2 Estimation of Color Shift

In this section, the color shift lifetime will be estimated, using the heat distribution result in section 7.1 and the regression model, which was established in Table 6-1.

For easy manipulation of numerical calculation, the temperature result of OLED panel calculated from the CFD analysis was transformed with matrix format of MATLAB program. Figure 7-4 shows that the color shift lifetime calculated with Equation (6.1) is 818.62 hours. In base of current thermal design and the reliability characteristics of OLED panel, the reliability of OLED display can be estimated at an early stage of product development.

7.3 Estimation of Luminance Degradation

Unlike the color shift lifetime, the regression model that enables the establishment of the relationship between the surface temperature of OLED panel and the performance of the luminance degradation was not clearly developed in this study. However, the acceleration factor of the luminance lifetime model was suggested in Equation (5.16) of section 5.1.1. Assuming that there is no acceleration condition about the initial luminance intensity, and the temperature under an

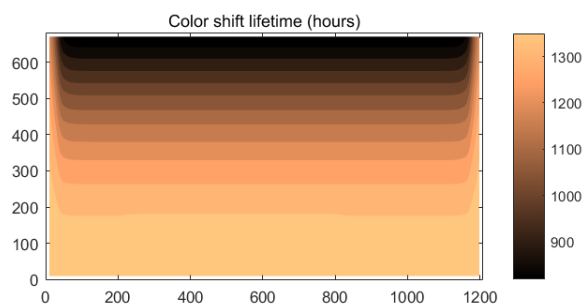

Figure 7-4 The estimated color shift lifetime.

accelerated condition, T_a, is directly related with the surface temperature of OLED panels, the relative luminance degradation is calculated as shown in Figure 7-5. Because the SED curve enables the estimation of luminance decay trend in the minimum temperature location, the luminance degradation at other location can be derived with the AF model by the temperature. As shown in Figure 7-5(d), the 50% degradation of the luminance appears after 1,850 hours. The time to failure of luminance was calculated as 1,823 hours by the linear interpolation of the relative luminance at 1,850 hours and at 1,800 hours.

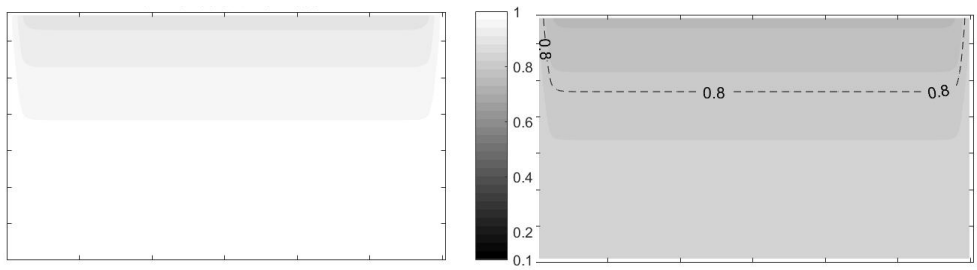

(a) Luminance distribution after 500 hours (b) Luminance distribution after 1,400 hours

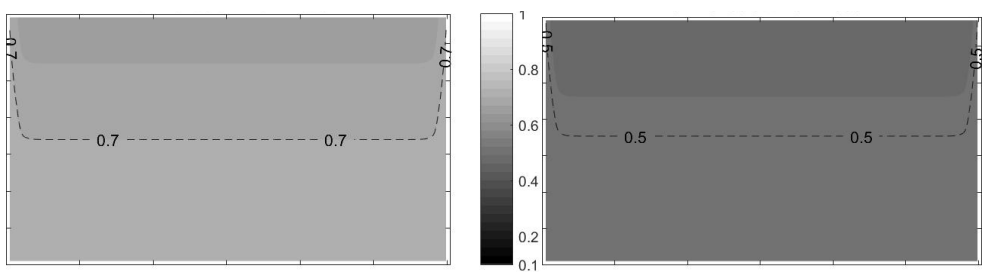

(c) Luminance distribution after 1,600 hours (d) Luminance distribution after 1,850 hours

Figure 7-5 The estimated luminance degradation from SED curve and AF by surface temperature.

Chapter 8. Contributions and Future Work

8.1 Contributions and Impacts

Large OLED panels with a size of 55 inches or larger are subjected to physical uncertainty in real-world applications (e.g., spatial temperature variations in the OLED panel and inherent randomness in organic materials). Estimation of the nominal lifetime of OLED panels is important for quality and reliability assurance during the design stage. Nevertheless, previous studies for OLEDs have not fully addressed these physical uncertainties to enable accurate lifespan estimation for large OLED panels. To fill this gap, in this research, we proposed (1) design of accelerated degradation tests (ADTs) for OLED panels, (2) development of two bivariate lifetime models for OLED panels, (3) a systematic scheme to build bivariate lifetime models for OLED panels, and (4) statistical model validation of the OLED surface temperature prediction model for OLED TV design using V&V methodology.

Contribution 1: Design of accelerated degradation tests for OLED panels

The display pattern in each TV set was suggested to predict two kinds of reliability issues – luminance degradation and color shift – for normal usage conditions and with results available within a short test period. An optimal design of

experiment was proposed by executing various accelerated conditions in each OLED panel. Six OLED panels proved to be enough to predict the lifetime during normal usage conditions.

Contribution 2: A novel bivariate lifetime model for luminance degradation

A novel bivariate lifetime model was proposed to analyze the lifespan testing data for OLEDs. The time to failure and time to 50% luminance degradation were calculated from the stretched exponential decay curve. The nominal life estimated using the bivariate lifetime model showed only a 4% error compared to the experimental data. The proposed bivariate lifetime model with the interaction term between the ambient temperature and the luminance intensity outperformed existing models. Thus, quality and reliability engineers are encouraged to use the bivariate lifetime model proposed in this study for OLEDs. Using the proposed model, the lifetime of large OLED panels subjected to normal usage conditions can be predicted by extrapolating accelerated life testing results from a manufacturer's own experiments.

Contribution 3: A novel bivariate lifetime model for color shift

In this work, a novel lifetime model was developed for large OLED panels that are subject to inherent randomness that includes variations in temperature and manufacturing tolerances. By estimating the parameters of the performance degradation curve, the time to 0.0322 color shift in the CIE 1931 coordinates was

calculated. A novel bivariate acceleration model was proposed to analyze the lifespan testing data for OLEDs. This model, combined with the BET model for initial luminance intensity and the Arrhenius relationship for ambient temperature, outperformed the previously published Intel and Peck models. The nominal life estimated using the proposed bivariate lifetime model showed only a 1% error compared to the experimental data.

Contribution 4: A systematic scheme to build bivariate lifetime models

A statistical approach was proposed to develop a lifetime model that considers the manufacturing and operational uncertainty sources in OLED panels. The proposed statistical analysis consists of: (1) estimation of the time to failure (TTF) using accelerated degradation data and the stretched exponential decay model, (2) inference of a common shape parameter for the lifetime distributions, (3) evaluation of validity through likelihood ratio analysis, and (4) prediction of lifetime distributions of OLED panels using the proposed bivariate AF model. This statistical approach will help predict an accurate lifetime distribution for large OLED panels subjected to various uncertainties, and will give guidance to OLED manufacturers for development of the lifetime model.

Contribution 5: Statistical validation of the bivariate lifetime models for OLED panels

A likelihood-ratio-based validation method was proposed to determine whether the common distribution parameter was significantly different from the individual distribution parameters estimated from lifespan testing data under the different acceleration levels. We demonstrated the applicability of the validation method using data from lifespan testing of OLEDs.

The goodness-of-fit test was utilized to evaluate the performance of the lifetime models. The proposed lifetime models were proven to estimate well the MTTFs of OLEDs in normal usage conditions.

Contribution 6: An analysis process for prediction of the color shift lifetime at an early stage of product development

The immature technology for the reliability estimation is a great hurdle for timely product development of OLEDs. Because there has been no way to estimate the color shift lifetime at an early stage of product development, while design changes are ongoing, mechanical engineers and reliability experts have traditionally had to execute many tests. To overcome this, a novel analysis process was suggested in this research.

The analysis process consists of: (1) a simple finite element model that enables incorporation of the uncertainty of the measured surface temperature, (2) statistical model validation that includes model calibration to demonstrate the agreement between the predicted results and a set of experimental data through the adjustment

of a set of physical input variables and a hypothesis test for validity checking to measure the degree of mismatch between the predicted and observed results, and (3) a regression model that can predict the color shift lifetime using the surface temperature calculated from the calibrated FE model.

In the early stages of product development, this process is expected to shorten the period of the product development, by predicting the color shift lifetime through simple heat dissipation analysis.

Based on these six achievements, we expect that the development period of both OLED panels and OLED TVs will be shortened. In addition, the research in this study can be utilized by manufacturers to find optimal designs to meet the criteria of the color shift lifetime at early stages of product development. The process during the product development will be innovated, as shown in Figure 8-1.

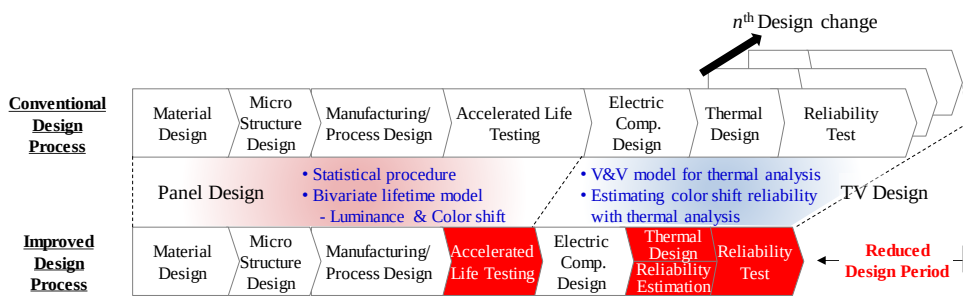

Figure 8-1 An improved design process by enabling concurrent engineering and reliability estimation.

8.2 Suggestions for Future Research

Future studies are needed to develop an advanced method that estimates multiple performance factors of OLED TVs using only temperature data at the early stages of development, not with respect to only a single performance measure. In addition, sensitivity analysis of various design parameters in OLED TVs must be studied to consider installation and dynamic operation conditions. Because OLED devices have only recently been commercialized, various acceleration factors related to installation locations and consumer's watching habits should be studied.

If necessary, prognostics-based qualification techniques for short qualification test times for highly reliable OLED devices can be employed to reduce the prediction errors and uncertainties. Ultimately, this research will provide design guidance that will enable designers and quality engineers to optimize the design of flexible and transparent OLED TVs.

References

[1] C. W. Han, K. M. Kim, S. J. Bae, H. S. Choi, J. M. Lee, T. S. Kim*, et al.*, "21.2: 55-inch FHD OLED TV employing New Tandem WOLEDs," in *SID Symposium Digest of Technical Papers*, 2012, pp. 279-281.

[2] M. K. Fung, Y. Q. Li, and L. S. Liao, "Tandem Organic Light-Emitting Diodes," *Advanced Materials,* vol. 28, pp. 10381-10408, 2016.

[3] H. Pang, L. Michalski, M. S. Weaver, R. Ma, and J. J. Brown, "Thermal behavior and indirect life test of large-area OLED lighting panels," *Journal of Solid State Lighting,* vol. 1, pp. 1-7, May 2014.

[4] J. Zhang, W. Li, G. Cheng, X. Chen, H. Wu, and M. H. Herman Shen, "Life prediction of OLED for constant-stress accelerated degradation tests using luminance decaying model," *Journal of Luminescence,* vol. 154, pp. 491-495, 2014.

[5] S. K. Ng, K. H. Loo, Y. M. Lai, and C. K. Tse, "Color control cystem for RGB LED with application to light sources suffering from prolonged aging," *IEEE Transaction on Industrial Electronics,* vol. 61, pp. 1788-1798, Apr. 2014.

[6] L. Han and N. Narendran, "An accelerated test method for predicting the useful life of an LED driver," *IEEE Transactions on Power Electronics,* vol. 26, pp. 2249-2257, 2011.

[7] J. Zhang, F. Liu, Y. Liu, H. Wu, W. Zhu, and W. Wu, "Life prediction for white OLED based on LSM under lognormal distribution," *Solid-State Electronics,* vol. 75, pp. 102-106, May 2012.

[8] H. Oh, S. Choi, K. Kim, B. D. Youn, and M. Pecht, "An empirical model to describe performance degradation for warranty abuse detection in portable electronics," *Reliability Engineering & System Safety,* vol. 142, pp. 92-99, Oct. 2015.

[9] H. Oh, H. P. Wei, B. Han, and B. D. Youn, "Probabilistic lifetime prediction of electronic packages using advanced uncertainty propagation and model calibration," *IEEE Transactions on Components, Packaging and Manufufacturing Technology,* vol. 6, No. 2, pp. 238-248, Feb. 2016.

[10] M. Nikulin, N. Limnios, N. Balakrishnan, W. Kahle, and C. Huber-Carol, "Reliability estimation of mechanical components using accelerated life testing models," in *Advances in Degradation Modeling*, 1st ed, New York: Springer Science & Business Media, 2010, pp. 253-260.

[11] J. Zhang, T. Zhou, H. Wu, Y. Liu, W. Wu, and J. Ren, "Constant-step-stress accelerated life test of white OLED under Weibull distribution case," *IEEE Transaction on Electron Devices,* vol. 59, pp. 715-720, Mar. 2012.

[12] F. K. Wang and T. P. Chu, "Lifetime predictions of LED-based light bars by accelerated degradation test," *Microelectronics Reliability,* vol. 52, pp. 1332-1336, 2012.

[13] J. I. Park and S. J. Bae, "Direct prediction methods on lifetime distribution of organic light-emitting diodes from accelerated degradation tests," *IEEE Transaction s Reliability,* vol. 59, pp. 74-90, Mar. 2010.

[14] C. Y. Peng, "Inverse Gaussian processes with random effects and explanatory variables for degradation data," *Technometrics,* vol. 57, pp. 100-111, 2015.

[15] Z. Pan and N. Balakrishnan, "Reliability modeling of degradation of products with multiple performance characteristics based on gamma processes," *Reliability Engineering & System Safety,* vol. 96, pp. 949-957, 2011.

[16] M. Guida and G. Pulcini, "The inverse Gamma process: A family of continuous stochastic models for describing state-dependent deterioration phenomena," *Reliability Engineering & System Safety,* vol. 120, pp. 72-79, 2013.

[17] Z. S. Ye, M. Xie, L. C. Tang, and N. Chen, "Semiparametric estimation of gamma processes for deteriorating products," *Technometrics,* vol. 56, pp. 504-513, 2014.

[18] J. Tang and T. S. Su, "Estimating failure time distribution and its parameters based on intermediate data from a Wiener degradation model," *Naval Research Logistics (NRL),* vol. 55, pp. 265-276, 2008.

[19] Z. S. Ye, Y. Wang, K. L. Tsui, and M. Pecht, "Degradation data analysis using Wiener processes with measurement errors," *IEEE Transactions on Reliability,* vol. 62, pp. 772-780, 2013.

[20] X. Wang and D. Xu, "An inverse Gaussian process model for degradation data," *Technometrics,* vol. 52, pp. 188-197, 2010.

[21] Z.-S. Ye and N. Chen, "The inverse Gaussian process as a degradation model," *Technometrics,* vol. 56, pp. 302-311, 2014.

[22] J. Luo, K. R. Pattipati, L. Qiao, and S. Chigusa, "Model-based prognostic techniques applied to a suspension system," *IEEE Transactions on Systems, Man, and Cybernetics-Part A: Systems and Humans,* vol. 38, pp. 1156-1168, 2008.

[23] F. Cadini, E. Zio, and D. Avram, "Model-based Monte Carlo state estimation for condition-based component replacement," *Reliability Engineering & System Safety,* vol. 94, pp. 752-758, 2009.

[24] M. Daigle, B. Saha, and K. Goebel, "A comparison of filter-based approaches for model-based prognostics," in *Aerospace conference, 2012 IEEE*, 2012, pp. 1-10.

[25] T. Sutharssan, C. Bailey, S. Stoyanov, and Y. Rosunally, "Prognostics and reliability assessment of light emitting diode packaging," in *Electronic Packaging Technology and High Density Packaging (ICEPT-HDP), 2011 12th International Conference on*, 2011, pp. 1-7.

[26] C. Hu, B. D. Youn, P. Wang, and J. T. Yoon, "Ensemble of data-driven prognostic algorithms for robust prediction of remaining useful life," *Reliability Engineering & System Safety,* vol. 103, pp. 120-135, 2012.

[27] B. Saha, K. Goebel, S. Poll, and J. Christophersen, "Prognostics methods for battery health monitoring using a Bayesian framework," *IEEE Transactions on instrumentation and measurement,* vol. 58, pp. 291-296, 2009.

[28] J. Fan, K.-C. Yung, and M. Pecht, "Prognostics of lumen maintenance for high power white light emitting diodes using a nonlinear filter-based approach," *Reliability Engineering & System Safety,* vol. 123, pp. 63-72, 2014.

[29] J. Fan, K. C. Yung, and M. Pecht, "Predicting long-term lumen maintenance life of LED light sources using a particle filter-based prognostic approach," *Expert Systems with Applications,* vol. 42, pp. 2411-2420, 2015.

[30] S. Chung, J. H. Lee, J. Jeong, J. J. Kim, and Y. Hong, "Substrate thermal conductivity effect on heat dissipation and lifetime improvement of organic light-emitting diodes," *Appllied Physics Letters,* vol. 94, p. 253302, Jun. 2009.

[31] F. K. Wang and Y. C. Lu, "Useful lifetime of white OLED under a constant stress accelerated life testing," *Optical and Quantum Electron.,* vol. 47, pp. 323-329, Mar. 2015.

[32] L. Pohl, E. Kollár, A. Poppe, and Z. Kohári, "Nonlinear electro-thermal modeling and field-simulation of OLEDs for lighting applications I: Algorithmic fundamentals," *Microelectron. J.,* vol. 43, pp. 624-632, Jul. 2012.

[33] M. Slawinski, D. Bertram, M. Heuken, H. Kalisch, and A. Vescan, "Electrothermal characterization of large-area organic light-emitting diodes employing finite-element simulation," *Organic Electronics,* vol. 12, pp. 1399-1405, 2011.

[34] A. Sure, K. R. Sarma, K. Paramanandam, R. H. Desai, A. Mukherjee, V. Baranwal,

et al., "Thermal modeling of organic light-emitting diode display panels," *Journal of Display Technology,* vol. 11, pp. 1048-1055, 2015.

[35] Z. Wen-Wen, W. Zhao-Xin, L. Ying-Wen, D. Jun, Y. Xue-Wen, and H. Xun, "Thermal Analysis of Organic Light Emitting Diodes Based on Basic Heat Transfer Theory," *Chinese Physics Letters,* vol. 32, p. 087201, 2015.

[36] J. S. Park, W.-J. Maeng, H.-S. Kim, and J.-S. Park, "Review of recent developments in amorphous oxide semiconductor thin-film transistor devices," *Thin Solid Films,* vol. 520, pp. 1679-1693, 2012.

[37] K.-Y. Lee and P.-P. Chao, "A new AMOLED pixel circuit with pulsed drive and reverse bias to alleviate OLED degradation," *IEEE Transactions on Electron Devices,* vol. 59, pp. 1123-1130, Apr. 2012.

[38] L. Yang, B. Wei, and J. Zhang, "Transient thermal characterization of organic light-emitting diodes," *Semiconductor Science and Technology,* vol. 27, p. 105011, 2012.

[39] M. Baldo and S. Forrest, "Transient analysis of organic electrophosphorescence: I. Transient analysis of triplet energy transfer," *Physical Review B,* vol. 62, 2000.

[40] W. E. Howard and O. F. Prache, "Microdisplays based upon organic light-emitting diodes," *IBM Journal of Research and Development,* vol. 45, pp. 115-127, 2001.

[41] M. Ishii and Y. Taga, "Influence of temperature and drive current on degradation mechanisms in organic light-emitting diodes," *Applied physics letters,* vol. 80, pp. 3430-3432, 2002.

[42] M. Ishii, "Luminance decay mechanisms in organic light-emitting diodes," *R&D Review of Toyota CRDL,* vol. 38, pp. 55-60, 2003.

[43] C. Sungjin and K. TaeHoon, "Symmetric current-balancing circuit for LED backlight with dimming," *IEEE Transactions on Industrial Electronics,* vol. 59, pp. 1698-1707, Apr. 2012.

[44] S.-M. Liu and Y.-C. Chou, "Color calibration for a surrounding true-color LED display system by PWM controls," *IEEE Transactions on Industrial Electronics,* vol. 61, pp. 6244-6252, Nov. 2014.

[45] I. 62341-6-1, "Organic light emitting diode (OLED) displays - Part 6-1: Measuring methods of optical and electro-optical parameters," ed, 2017.

[46] K. Sugimoto, T. Yoshioka, H. Kijima, H. Ohata, S. Miyaguchi, T. Tsutsui*, et al.*, "P-162: Accelerated Lifetime Testing of White OLED Panels for Lighting," in *SID*

Symposium Digest of Technical Papers, San Francisco, CA, 2016, pp. 1730-1733.

[47] L. Y. Chen, S. H. Chen, S. J. Dai, C. T. Kuo, and H. C. Wang, "Spectral design and evaluation of OLEDs as light sources," *Organic Electronics,* vol. 15, pp. 2194-2209, 2014.

[48] Y. h. Jang, K. t. Kim, H. m. Lee, J. e. Lee, J. h. Kim, C. s. Oh*, et al.*, "Experimental study for the establishment of an evaluation criterion for the image sticking effect in OLED TV panels," *Journal of the Society for Information Display,* vol. 24, pp. 569-575, 2016.

[49] Z. Kohári, E. Kollár, L. Pohl, and A. Poppe, "Nonlinear electro-thermal modeling and field-simulation of OLEDs for lighting applications II: Luminosity and failure analysis," *Microelectronics Journal,* vol. 44, pp. 1011-1018, 2013.

[50] W. L. Oberkampf, T. G. Trucano, and C. Hirsch, "Verification, validation, and predictive capability in computational engineering and physics," *Applied Mechanics Reviews,* vol. 57, pp. 345-384, 2004.

[51] ASME, "Guide for verification and validation in computational solid mechanics," New York, NY,2006.

[52] W. L. Oberkampf and T. G. Trucano, "Verification and validation in computational fluid dynamics," *Progress in Aerospace Sciences,* vol. 38, pp. 209-272, 2002.

[53] B. H. Thacker, S. W. Doebling, F. M. Hemez, M. C. Anderson, J. E. Pepin, and E. A. Rodriguez, "Concepts of model verification and validation," Los Alamos National Lab., Los Alamos, NM (US)2004.

[54] R. W. Logan and C. K. Nitta, "Verification & validation (V&V) methodology and quantitative reliability at confidence (QRC): basis for an investment strategy," *Lawrence Livermore National Laboratory, UCRL-ID-150874,* vol. 12, p. 30, 2002.

[55] I. Babuska and J. T. Oden, "Verification and validation in computational engineering and science: basic concepts," *Computer Methods in Applied Mechanics and Engineering,* vol. 193, pp. 4057-4066, 2004.

[56] C. Kaner and J. Falk, *Testing computer software*: Wiley, 1999.

[57] P. J. Roache, "Verification of codes and calculations," *AIAA journal,* vol. 36, pp. 696-702, 1998.

[58] W. L. Oberkampf and M. F. Barone, "Measures of agreement between computation and experiment: validation metrics," *Journal of Computational Physics,* vol. 217,

pp. 5-36, 2006.

[59] S. Ferson, W. L. Oberkampf, and L. Ginzburg, "Model validation and predictive capability for the thermal challenge problem," *Computer Methods in Applied Mechanics and Engineering,* vol. 197, pp. 2408-2430, 2008.

[60] R. Rebba and J. Cafeo, "Probabilistic analysis of a static frame model," *Computer Methods in Applied Mechanics and Engineering,* vol. 197, pp. 2561-2571, 2008.

[61] B. D. Youn, B. C. Jung, Z. Xi, S. B. Kim, and W. Lee, "A hierarchical framework for statistical model calibration in engineering product development," *Computer Methods in Applied Mechanics and Engineering,* vol. 200, pp. 1421-1431, 2011.

[62] B. C. Jung, H. Yoon, H. Oh, G. Lee, M. Yoo, B. D. Youn*, et al.*, "Hierarchical model calibration for designing piezoelectric energy harvester in the presence of variability in material properties and geometry," *Structural and Multidisciplinary Optimization,* vol. 53, pp. 161-173, 2016.

[63] K. Campbell, "Statistical calibration of computer simulations," *Reliability Engineering & System Safety,* vol. 91, pp. 1358-1363, 2006.

[64] A. Calvi, "Uncertainty-based loads analysis for spacecraft: Finite element model validation and dynamic responses," *Computers & structures,* vol. 83, pp. 1103-1112, 2005.

[65] M. C. Kennedy and A. O'Hagan, "Bayesian calibration of computer models," *Journal of the Royal Statistical Society: Series B (Statistical Methodology),* vol. 63, pp. 425-464, 2001.

[66] Z. Jiang, W. Chen, Y. Fu, and R.-J. Yang, "Reliability-based design optimization with model bias and data uncertainty," *SAE International Journal of Materials and Manufacturing,* vol. 6, pp. 502-516, 2013.

[67] K. Farrell, J. T. Oden, and D. Faghihi, "A Bayesian framework for adaptive selection, calibration, and validation of coarse-grained models of atomistic systems," *Journal of Computational Physics,* vol. 295, pp. 189-208, 2015.

[68] Y. Xiong, W. Chen, K.-L. Tsui, and D. W. Apley, "A better understanding of model updating strategies in validating engineering models," *Computer methods in applied mechanics and engineering,* vol. 198, pp. 1327-1337, 2009.

[69] J. P. Kleijnen, *Statistical tools for simulation practitioners*: Marcel Dekker, Inc., 1986.

[70] D. C. Montgomery, "Design and Analysis of Experiments, John Wiley & Sons," *New York,* pp. 64-65, 2001.

[71] P. Varghese, R. N. Braswell, B. Wang, and C. Zhang, "Statistical tolerance analysis using FRPDF and numerical convolution," *Computer-Aided Design,* vol. 28, pp. 723-732, 1996.

[72] C. Y. Lin, W. H. Huang, M. C. Jeng, and J. L. Doong, "Study of an assembly tolerance allocation model based on Monte Carlo simulation," *Journal of Materials Processing Technology,* vol. 70, pp. 9-16, 1997.

[73] I. M. Sobol, "On quasi-monte carlo integrations," *Mathematics and Computers in Simulation,* vol. 47, pp. 103-112, 1998.

[74] Y. T. Wu, "Computational methods for efficient structural reliability and reliability sensitivity analysis," *AIAA journal,* vol. 32, pp. 1717-1723, 1994.

[75] P. Bjerager, "Probability integration by directional simulation," *Journal of Engineering Mechanics,* vol. 114, pp. 1285-1302, 1988.

[76] D. H. Jung and B. C. Lee, "Development of a simple and efficient method for robust optimization," *International Journal for Numerical Methods in Engineering,* vol. 53, pp. 2201-2215, 2002.

[77] S. Rahman and B. Rao, "A perturbation method for stochastic meshless analysis in elastostatics," *International Journal for Numerical Methods in Engineering,* vol. 50, pp. 1969-1991, 2001.

[78] F. Yamazaki, A. Member, M. Shinozuka, and G. Dasgupta, "Neumann expansion for stochastic finite element analysis," *Journal of Engineering Mechanics,* vol. 114, pp. 1335-1354, 1988.

[79] T. W. Simpson, T. M. Mauery, J. J. Korte, and F. Mistree, "Kriging models for global approximation in simulation-based multidisciplinary design optimization," *AIAA journal,* vol. 39, pp. 2233-2241, 2001.

[80] G. G. Wang and S. Shan, "Review of metamodeling techniques in support of engineering design optimization," *Journal of Mechanical design,* vol. 129, pp. 370-380, 2007.

[81] R. Jin, W. Chen, and T. W. Simpson, "Comparative studies of metamodelling techniques under multiple modelling criteria," *Structural and multidisciplinary optimization,* vol. 23, pp. 1-13, 2001.

[82] S. Rahman and H. Xu, "A univariate dimension-reduction method for multi-dimensional integration in stochastic mechanics," *Probabilistic Engineering Mechanics,* vol. 19, pp. 393-408, 2004.

[83] B. D. Youn, K. K. Choi, and K. Yi, "Performance moment integration (PMI) method for quality assessment in reliability-based robust design optimization," *Mechanics Based Design of Structures and Machines,* vol. 33, pp. 185-213, 2005.

[84] H. Xu and S. Rahman, "A generalized dimension-reduction method for multidimensional integration in stochastic mechanics," *International Journal for Numerical Methods in Engineering,* vol. 61, pp. 1992-2019, 2004.

[85] B. C. Jung, J. Park, H. Oh, J. Kim, and B. D. Youn, "A framework of model validation and virtual product qualification with limited experimental data based on statistical inference," *Structural and Multidisciplinary Optimization,* vol. 51, pp. 573-583, Oct. 2015.

[86] B. D. Youn and Z. Xi, "An Effective Random Field Characterization for Probability Analysis and Design," in *Proceedings of 49th AIAA/ASME/ASCE/AHS/ASC Structures, Structural Dynamics, and Materials Conference*, 2008.

[87] B. D. Youn, Z. Xi, and P. Wang, "Eigenvector dimension reduction (EDR) method for sensitivity-free probability analysis," *Structural and Multidisciplinary Optimization,* vol. 37, pp. 13-28, 2008.

[88] T. Nagayama, T. Yamamoto, T. Nakamura, and Y. Mizutani, "Fabrication of low CTE metal masks by the Invar Fe-Ni alloy electroforming process for large and fine pitch OLED displays," *ECS Transactions,* vol. 50, pp. 117-122, 2013.

[89] J. Heo, H. Min, and M. Lee, "Laser micromachining of permalloy for fine metal mask," *International Journal of Precision Engineering and Manufacturing-Green Technology,* vol. 2, pp. 225-230, 2015.

[90] J. P. Spindler and T. K. Hatwar, "8.2: Development of Tandem White Architecture for Large-Sized AMOLED Displays with Wide Color Gamut," in *SID Symposium Digest of Technical Papers*, 2007, pp. 89-92.

[91] J. W. Hamer, A. D. Arnold, M. L. Boroson, M. Itoh, T. K. Hatwar, M. J. Helber*, et al.*, "System design for a wide-color-gamut TV-sized AMOLED display," *Journal of the Society for Information Display,* vol. 16, pp. 3-14, 2008.

[92] J. P. Spindler and T. K. Hatwar, "Fluorescent-based tandem white OLEDs designed for display and solid-state-lighting applications," *Journal of the Society for Information Display,* vol. 17, pp. 861-868, 2009.

[93] C. W. Han, Y. H. Tak, and B. C. Ahn, "15-in. RGBW panel using two-stacked white OLED and color filters for large-sized display applications," *Journal of the Society for Information Display,* vol. 19, pp. 190-195, 2011.

[94] D. L. MacAdam, "Visual sensitivities to color differences in daylight," *JOSA,* vol. 32, pp. 247-274, 1942.

[95] The Department of Energy, "ENERGY STAR® Program Requirements for CFLs Partner Commitments," ed, 2007. [Online]. Available: https://www.energystar.gov/ia/partners/prod_development/revisions/downloads/cfls/Criteria_CFLs_Version4.0_draft4.pdf

[96] M. Wood, "MacAdam ellipses," *Out of the Wood, Mike Wood Consulting LLC.(retrieved on Jun. 8, 2011). Retrieved from the internet: URL: http://www. mikewoodconsulting. com/articles/Protocol% 20Fall,* vol. 202010, 2010.

[97] H. J. Shin, S. Takasugi, K. M. Park, S. H. Choi, Y. S. Jeong, H. S. Kim*, et al.*, "50.1: Invited paper: Technological progress of panel design and compensation methods for large-size UHD OLED TVs," in *SID Symp. Dig. of Tech. Pap.*, San Diego, CA, 2014, pp. 720-723.

[98] V. C. Bender, T. B. Marchesan, and J. M. Alonso, "Solid-state lighting: A concise review of the state of the art on LED and OLED modeling," *IEEE Industrial Electronics Magazine,* vol. 9, pp. 6-16, Jun. 2015.

[99] C. H. Oh, H. J. Shin, W. J. Nam, B. C. Ahn, S. Y. Cha, and S. D. Yeo, "21.1: Invited paper: Technological progress and commercialization of OLED TV," in *SID Symp. Digest of Technical Paper*, 2013, pp. 239-242.

[100] D. Kondakov, W. Lenhart, and W. Nichols, "Operational degradation of organic light-emitting diodes: Mechanism and identification of chemical products," *Journal of Applied Physics,* vol. 101, 024512, 2007.

[101] B. W. Chen, T. C. Chang, Y. J. Hung, T. Y. Hsieh, M. Y. Tsai, and P. Y. Liao, "Investigation of temperature-dependent asymmetric degradation behavior induced by hot carrier effect in oxygen ambiance in In–Ga–Zn-O thin film transistors," *Thin Solid Films,* vol. 572, pp. 33-38, Oct. 2014.

[102] X. Yang, X. Xu, and G. Zhou, "Recent advances of the emitters for high performance deep-blue organic light-emitting diodes," *Journal of Materials Chemistry C,* vol. 3, pp. 913-944, 2015.

[103] L. Liao, K. P. Klubek, and C. W. Tang, "High-efficiency tandem organic light-emitting diodes," *Applied physics letters,* vol. 84, pp. 167-169, 2004.

[104] Cascaded organic electroluminescent devices with improved voltage stability by L. S. Liao, K. P. Klubek, D. L. Comfort, and C. W. Tang. (6. Apr. 2004). U.S. Patent No 6,717,358 B1 [Online] Available: https://www.google.com/patents/US6717358.

[105] C. Féry, B. Racine, D. Vaufrey, H. Doyeux, and S. Cinà, "Physical mechanism responsible for the stretched exponential decay behavior of aging organic light-emitting diodes," *Applied Physics Letters,* vol. 87, 2005.

[106] P. Burrows, V. Bulovic, S. Forrest, L. S. Sapochak, D. McCarty, and M. Thompson, "Reliability and degradation of organic light emitting devices," *Applied Physics Letters,* vol. 65, pp. 2922-2924, 1994.

[107] B. M. Weon, S. Y. Kim, J.-L. Lee, and J. H. Je, "Evolution of luminance by voltage in organic light-emitting diodes," *Applied Physics Letters,* vol. 88, p. 013503, 2006.

[108] K. Trachenko and M. T. Dove, "Local events and stretched-exponential relaxation in glasses," *Physical Review B,* vol. 70, p. 132202, 2004.

[109] A. Cester, D. Bari, J. Framarin, N. Wrachien, G. Meneghesso, S. Xia*, et al.*, "Thermal and electrical stress effects of electrical and optical characteristics of Alq3/NPD OLED," *Microelectronics Reliability,* vol. 50, pp. 1866-1870, Aug. 2010.

[110] J. Buytaert, J. Bleumers, A. Steen, and P. Hanselaer, "Optical determination of the junction temperature of OLEDs," *Organic Electronics,* vol. 14, pp. 2770-2776, Aug. 2013.

[111] D. J. Klinger, "Humidity acceleration factor for plastic packaged electronic devices," *Quality and Reliability Engineering International,* vol. 7, pp. 365-370, 1991.

[112] D. S. Peck, "Comprehensive model for humidity testing correlation," in *Reliability Physics Symposium, 1986. 24th Annual*, 1986, pp. 44-50.

[113] Panasonic. (2012). *Accelerated life test*. Available: http://www.semicon.panasonic.co.jp/en/aboutus/reliability.html

[114] L. A. Escobar and W. Q. Meeker, "A Review of Accelerated Test Models," *Statistical Science,* vol. 21, pp. 552-577, 2006.

[115] D. K. Flattery, C. R. Fincher, D. L. LeCloux, M. B. O'Regan, and J. S. Richard, "Clearing the road to mass production of OLED television," *Information Display,* vol. 10, pp. 8-13, Oct. 2011.

[116] J. Zhang, C. Wang, X. Chen, G. Cheng, Y. Qiu, and M. H. Shen, "Experimental test

and life estimation of the OLED at normal working stress based on the luminance degradation model," *Luminescence,* vol. 30, pp. 371-375, Jul. 2015.

[117] W. B. Nelson, "Likelihood ratio test," in *Accelerated Testing: Statistical Models, Test Plans, and Data Analysis*, 3rd ed Hoboken, New Jersey: John Wiley & Sons, 2009, pp. 475-480.

[118] S. Scholz, D. Kondakov, B. r. Lüssem, and K. Leo, "Degradation Mechanisms and Reactions in Organic Light-Emitting Devices," *Chemical reviews,* vol. 115, pp. 8449-8503, 2015.

[119] Y. Kim and H. Lee, "Voltage-programmed AM-OLED pixel circuit to compensate threshold voltage and mobility variations," *Electronics Letters,* vol. 49, pp. 796-798, 2013.

[120] R. Shringarpure, S. Venugopal, L. T. Clark, D. R. Allee, and E. Bawolek, "Localization of gate bias induced threshold voltage degradation in a-Si: H TFTs," *Electron Device Letters, IEEE,* vol. 29, pp. 93-95, 2008.

[121] Y. Morimoto, Y. Jinno, K. Hirai, H. Ogata, T. Yamada, and K. Yoneda, "Influence of the Grain Boundaries and Intragrain Defects on the Performance of Poly-Si Thin Film Transistors," *Journal of The Electrochemical Society,* vol. 144, pp. 2495-2501, 1997.

[122] X. Chen, B. Liu, Y. Chen, M. Zhao, C. J. Xue, and X. Guo, "Active compensation technique for the thin-film transistor variations and OLED aging of mobile device displays," presented at the Proceedings of the International Conference on Computer-Aided Design, San Jose, California, 2012.

[123] V. C. Bender, N. D. Barth, F. B. Mendes, R. A. Pinto, T. B. Marchesan, and J. M. Alonso, "Electrical characterization and modeling of Organic Light-Emitting Diodes (OLEDs)," in *Industrial Electronics (ISIE), 2015 IEEE 24th International Symposium on*, 2015, pp. 1190-1195.

[124] J. C. Sturm, W. Wilson, and H. Iodice, "Thermal effects and scaling in organic light-emitting flat-panel displays," *IEEE Journal of selected topics in quantum electronics,* vol. 4, pp. 75-82, 1998.

[125] Y. Zhu and N. Narendran, "A spectral measurement method for determining white OLED average junction temperatures," 2016, pp. 995405-995405-7.

[126] J. Choi, W. Lee, J. Park, and B. Youn, "A study on robust design optimization of layered plate bonding process considering uncertainties," *Structural and Multidisciplinary Optimization,* vol. 35, pp. 531-540, 2008.

[127] H. Oh, H.P. Wei, B. Han, and B. D. Youn, "Probabilistic Lifetime Prediction of Electronic Packages Using Advanced Uncertainty Propagation Analysis and Model Calibration," *IEEE Transactions on Components, Packaging and Manufacturing Technology,* vol. 6, pp. 238-248, 2016.

[128] H. Oh, J. Kim, H. Son, B. D. Youn, and B. C. Jung, "A systematic approach for model refinement considering blind and recognized uncertainties in engineered product development," *Structural and Multidisciplinary Optimization,* vol. 54, pp. 1527-1541, 2016.

Abstract (Korean)

유기 발광 디스플레이 수명 모델 제안 및 모델 검증 체계 연구

김 대 환
서울대학교 대학원
기계항공공학부

액정 디스플레이에 비해 OLED 디스플레이의 여러 장점에도 불구하고 휘도 열화나 색좌표 변경과 같은 디스플레이 신뢰성에 대한 우려가 있다. 특히 대형 OLED 디스플레이 (55 인치 혹은 그 이상의 디스플레이)의 수명을 정확히 추정하기 위한 시험 기술이 정립되어 있지 않다. 제한된 시편수와 성숙하지 못한 기술력은 적기의 제품개발에 많은 장애 요소가 되고 있다.

본 연구에서는 대형 OLED 디스플레이의 불확실성을 잘 반영하고 실사용 조건의 수명을 정확히 예측할 수 있는 통계적인 접근방법을 제시하고자 한다. 제안하고 있는 통계적인 해석 절차는 (1) 가속 열화 시험법의 설계, (2) OLED 패널의 이항 수명모델을 개발할 수 있는 체계적인 절차, (3) OLED 패널의 이항 수명식의 개발, (4) OLED TV 설계를 위한 OLED 표면 온도예측 모델의 통계적인 모델 검정으로 구성되어 있다. 이런 통계적인 접근은 다양한 불확실성을 가진 대형 OLED 패널의 정확한 수명 분포를 예측하고 요구 수명을 만족할 수 있는 OLED TV 설계에 활용가능 하리라고 본다.

앞서 언급한 두개의 이항 수명모델은 제조공정이나 동작 중의 다양한 불확실성을 감안하여 실사용 조건의 대형 OLED 패널의 수명을

정확하게 예측하기위해 제안하고자 한다. 이항 가속모델은 두개의 주요 인자인 주위 온도와 초기 휘도값을 고려하고 있다. 첫번째는 제품 휘도의 열화 특성을 예측하는 모델이고, 다른 하나는 색좌표의 열화 특성을 예측하는 모델로써 예측된 수명값과 실제 수명 시험결과가 잘 일치하고 있음을 근거로 수명 모델의 성능을 제시한다.

색좌표 수명을 보증하는 일은 적기의 제품개발에 있어서 가장 큰 걸림돌이다. 하지만 제품개발 초기에 설계 변경에 따른 색좌표 수명을 예측할 수 있는 효과적인 방법이 현존하지 않다. 본 연구에서는 색좌표 수명 분석을 위한 새로운 방법을 제시하였다. 이는 (1) 측정된 표면온도의 불확실성을 잘 표현할 수 있는 유한요소 모델, (2) 일련의 물리적 입력 변수의 조절을 통해 실험 결과와 예측 결과를 잘 일치시켜주는 모델 보정 기법과 예측 결과와 측정된 결과와의 차이 정도를 유의한지 판단하는 가설검정, (3) 제품개발 초기에 표면온도를 활용하여 색좌표 수명을 예측할 수 있는 회귀모델로 구성되어 있다. 이는 제품개발 초기에 방열해석을 통해 색좌표 수명을 예측함으로써 제품개발 기간을 단축시킬 것으로 기대 된다.

주제어 : 유기발광소자
가속 열화 시험
수명 모델
색좌표 변화
통계적 모델 보정

학 번 : 2011-30198